



Design, synthesis and evaluation of new quinazolin-4-one derivatives as apoptotic enhancers and autophagy inhibitors with potent antitumor activity



Heba S.A. ElZahabi ^a, Mohamed S. Nafie ^{b,1}, Dina Osman ^{c,1}, Nehal H. Elghazawy ^d, Dalia H. Soliman ^a, Abdelghany Ali H. EL-Helby ^e, Reem K. Arafa ^{d,f,*}

^a Department of Medicinal and Pharmaceutical Chemistry, Faculty of Pharmacy, Al-Azhar University, Girls Branch, Cairo, Egypt

^b Chemistry Department, Faculty of Science, Suez Canal University, Ismailia, 41522, Egypt

^c Pharmaceutical Chemistry Department, Faculty of Pharmacy, MSA University, Egypt

^d Drug Design and Discovery Lab, Zewail City of Science and Technology, Giza, 12578, Egypt

^e Department of Pharmaceutical Chemistry, Faculty of Pharmacy, Al-Azhar University, Boys Branch, Cairo, Egypt

^f Biomedical Sciences Program, University of Science and Technology, Zewail City of Science and Technology, Giza, 12578, Egypt

ARTICLE INFO

Article history:

Received 6 February 2021

Received in revised form

29 May 2021

Accepted 30 May 2021

Available online 5 June 2021

Keywords:

Quinazolin-4-ones

Breast cancer

EGFR

Cell cycle analysis

Apoptosis

Autophagy

ABSTRACT

This work presents the design and synthesis of a series of new quinazolin-4-one derivatives, based on the established effectiveness of quinazoline-based small molecules as anticancer agents. Synthesized compounds were more potent against MCF-7 than A-549 with low to submicromolar IC₅₀s. Compound **17** exhibited the best IC₅₀ being equipotent with the positive control doxorubicin (IC₅₀ = 0.06 μM) and better than 5-fluorouracil (IC₅₀ = 2.13 μM). Compound **17** was further tested against MDA-MB-231 and MCF-10A and was found to be > 2 folds more cytotoxic on MCF-7. Significant apoptotic activity was elicited by **17** on MCF-7 where it increased apoptotic cell death along with induction of pre-G1 and G1-phase cell cycle arrest. Similarly, **17** was able to induce apoptosis in MD-MB-231 treated cells associated with a disruption of the cell cycle causing arrest at the pre-G1 and S phases. Investigation of gene expression in MCF-7 demonstrated an increased expression of the proapoptotic genes P53, PUMA, Bax, caspases 3, 8 and 9 and a decrease of the anti-apoptotic gene Bcl2. Also, **17** reduced autophagy giving way for apoptosis to induce cancer cells death. This latter observation was associated with downregulation of EGFR and its downstream effectors PI3K, AKT and mTor. As its biomolecular target, **17** also inhibited EGFR similar to erlotinib (IC₅₀ = 0.072 and 0.087 μM, respectively). Additionally, *in vivo* testing in a mouse model of breast cancer affirmed the anti-tumor efficacy of **17**. Finally, docking of **17** against EGFR ATP binding site demonstrated its ability to bind with EGFR resembling erlotinib.

© 2021 Elsevier Masson SAS. All rights reserved.

1. Introduction

Cancer is a multifactorial complex disorder that involves abnormal cell growth with potential to invade and transfer other parts of the body. According to Globocan 2020, the global estimate of cancer cases is 19.3 million cases and 10 million cancer deaths in 2020. Consequently, cancer research is expanding over the years in hope of reaching significant advances in the fields of its diagnosis

and treatment [1]. No matter how advanced the techniques for cancer treatments are, continuous search for new anticancer molecules remains essential owing to matters associated with selectivity, potency and drug resistance.

For discovery of new anticancer moieties, the search for small molecules with definite target is requested regularly. Medicinal chemistry field was able to introduce many heterocyclic moieties covering extensive area of chemical space qualifying them as magnificent starting points for developing anticancer agents. Accordingly, the FDA has approved over 100 anticancer agents over the past 50 years [2]. Due to wide prevalence in nature, heterocycles are pretty much the main scaffold of all these anticancer compounds which can interact with different targets involved in

* Corresponding author. Zewail City of Science and Technology, Ahmed Zewail Road October Gardens, Giza, 12578, Egypt.

E-mail address: rkhidr@zewailcity.edu.eg (R.K. Arafa).

¹ Authors with equal contribution.

cancer progression [3]. Quite some of these approved anticancer agents are based on quinazoline as their main scaffold [4].

Many quinazoline-based APIs were granted FDA approval and are in clinical use for cancer management such as Erlotinib, Gefitinib and Lapatinib (Fig. 1) [5]. On a molecular level, those drugs elicit their chemotherapeutic action by virtue of being potent epidermal growth factor receptor (EGFR)-targeted agents. Additionally, quinazolin-4-one derivatives have proven active against multiple types of cancer with noticeable variability in their mechanism of action [6–11].

Anticancer activity of quinazoline-based cytotoxic agents is mostly associated with alterations in cell cycle progression, induction of apoptosis and modification of autophagy. The effect of autophagy on cancer cells is still a matter of duality. At early tumorigenesis autophagy suppresses cancer cells survival and induce cell death, but at later stages it becomes pro-tumorigenic by promoting allowing cancer cells survival under stressful conditions of hypoxia helping them meet demanding metabolic needs thus promoting proliferation, tumor growth [12–16]. It was reported that mammary tumors for example benefit from autophagy as it mitigates metabolic stress and gene damage as well as induce chemotherapy resistance [14–16]. Thus, new quinazolin-4-one-based chemotherapeutics regulating autophagy are being widely explored (e.g. MJ-33 and DQQ, Fig. 1) [17,18].

Additionally, it has been demonstrated that there exists a cross talk between EGFR and autophagy. EGFR signaling plays a pleotropic role in regulation of autophagy where it can either suppresses or promote the autophagic response through two axes downstream of EGFR. The PI3K/AKT1 axis activates mTOR, and eventually inhibits autophagy [19] while EGFR-mediated RAS signaling activation would promote autophagy [20]. EGFR-tyrosine kinase inhibitors (TKIs) were found to induce stress conditions to

cancer cells with subsequent activation of protective autophagy in multiple cancers [21,22] thus leading to refractory response to EGFR-TKIs and development of resistance enhanced cancer cell survival and poor prognosis [23–25]. Thus, targeting both EGFR and autophagy can represent a logical combination for attaining better results in cancer treatment. In fact, co-inhibition of EGFR signaling and autophagy has demonstrated significant therapeutic effectiveness [24–27].

In line with our previous attempts to explore new scaffolds that act as anticancer agents [28–35], we herein report design and synthesis of a new series of quinazolin-4-one backbone based molecules (Fig. 1). From a structure-activity relationship (SAR) perspective, the design of our compounds aimed at focusing on the introduction of a variety of substituents at positions 2 and 3 of the 6,8-dibromoquinazolin-4-one ring system to be able to study the SAR of this series. The groups added were varied between aliphatic and aromatic, electron withdrawing and electron donating as well as hydrogen bond donating and/or accepting characters. The antiproliferative biological effect of all the synthesized compounds were assessed against MCF-7 human breast cancer cell lines and A-549 lung cancer cell line, with additional specific testing against MDA-MB-231 and MCF-10A. A serious of *in vitro* and *in vivo* assays were also conducted on the most active representative of this class to investigate its effect on apoptosis, cell cycle alteration, autophagy and EGFR inhibition and expression of EGFR and related genes. Finally docking was performed to predict the possible binding mode of a member of this class to their bio-target EGFR.

2. Results and discussion

2.1. Chemistry

The synthesis pathway adopted for preparation of the target compounds in this study are depicted in Schemes 1–4.

Scheme 1 outlines the synthesis of the key synthetic intermediate of this project, 6,8-dibromo-2-methylquinazolin-4(3H)-one **4**, from the starting material 2-aminobenzoic acid **1** in three steps. First, an acetic acid solution of 2-aminobenzoic acid-anthranilic acid- (**1**) was treated with bromine solution to give 2-amino-4,6-dibromobenzoic acid **2**. This procedure has been modified from the original suggestion of Oates et al. for obtaining the 3,5 dibromoanthranilic acid [36]. Reflux of the 4,6-dibromo-anthranilic acid **2** in acetic anhydride furnished 6,8-dibromo-2-methyl-4H-benzo[d][1,3]oxazin-4-one **3** which was finally converted to **4** through refluxing in ethanol in the presence of concentrated ammonia [37].

Intermediate **4** was then deployed in three different schemes to obtain the target compounds. Scheme 2 depicts the synthesis of quinazolin-4-ones **5a-c**, **6-11**, **12a-c** and **13**. First, acetanilide derivatives **5a-c** were prepared by reacting **4** with the appropriate corresponding chloroacetanilides in dry acetone in the presence of anhydrous potassium carbonate. Second, compound **4** was allowed to react with ethyl chloroacetate in dry acetone in the presence of anhydrous K₂CO₃ to yield the ethyl acetate derivative **6** which was then refluxed with hydrazine hydrate in absolute ethanol to give the hydrazide counterpart **7** [38]. Compound **7** is a major intermediate for the synthesis of derivatives **8**, **9**, **10**, **11**, **12a-c** and **13**. The pyrazolyl quinazolin-4-one **8** was obtained by reflux of mixture of the hydrazide **7** and ethyl acetoacetate in ethanol for 6 h [39]. Similarly, the analogous pyrazolyl derivatives **9** and **10** were obtained as result of reflux of **7** with ethyl cyanoacetate and carbon-disulfide, respectively. On the other hand, thiosemicarbazide derivative **11** was obtained by treating **7** with phenyl isothiocyanate. Whereas Schiff's bases **12a-c** were the products of reaction of **7** with the corresponding benzaldehydes [40]. Finally, compound

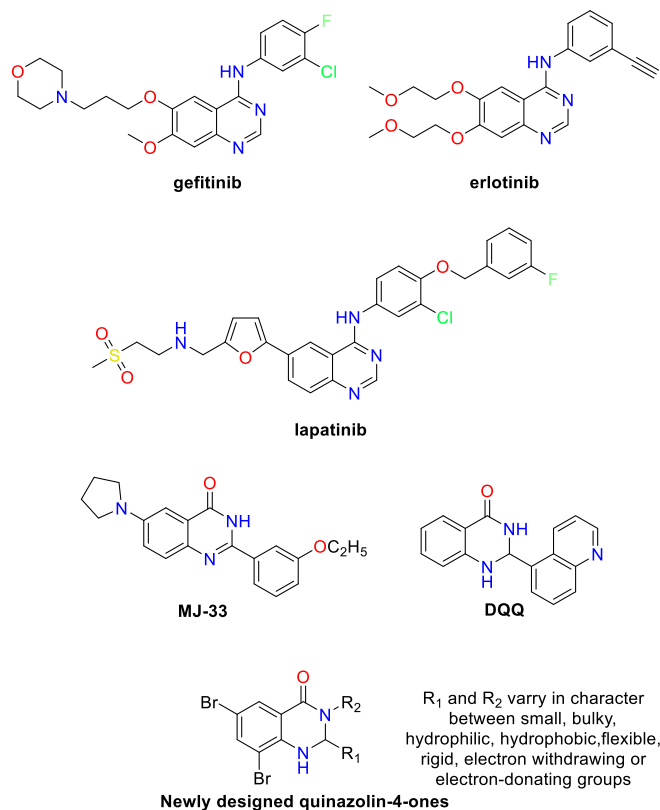
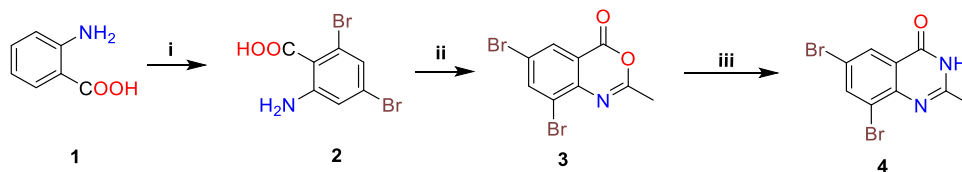
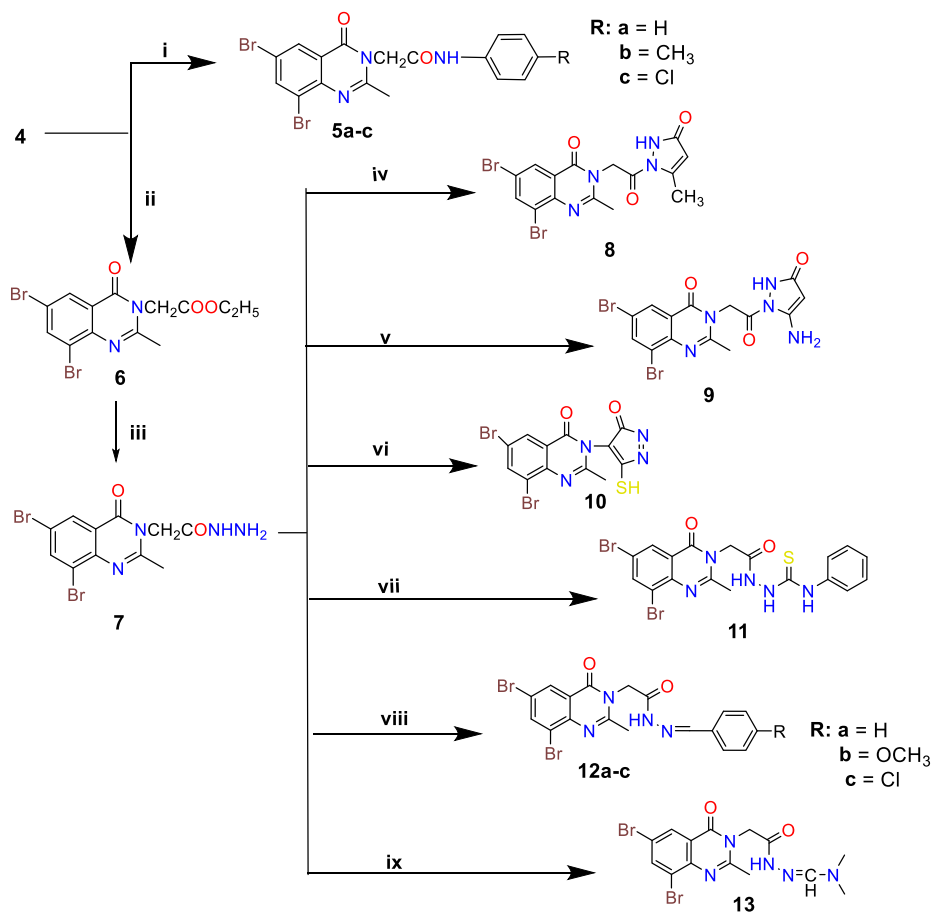


Fig. 1. Structures of some quinazoline based anticancer agents and designed target compounds.



Reagent and conditions: i) Br₂, Glacial acetic acid, rt, 5h ; ii) Acetic anhydride, reflux, 3h; iii) Abs. Ethanol, conc. Ammonia, reflux, 3h

Scheme 1. Synthesis of the key intermediate **4**.



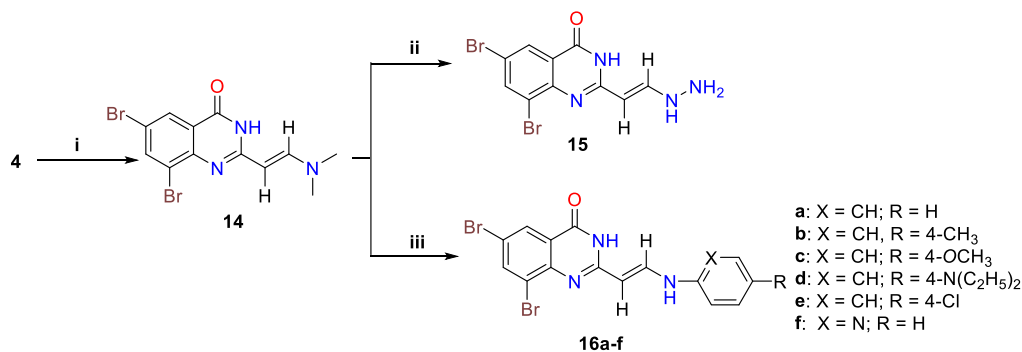
Reagent and conditions: i) Substituted 2-chloro-*N*-phenylacetamide derivative, anhyd. K₂CO₃, dry acetone, reflux, 12h; ii) Ethyl chloroacetate, Anhyd. K₂CO₃, Abs. Ethanol, reflux, 5h; iii) 99% NH₂NH₂, Abs. Ethanol, reflux, 12h; iv) Ethyl acetoacetate, Abs. Ethanol, reflux, 6h; v) Ethyl cyanoacetate, Abs. Ethanol, reflux, 6h; vi) CS₂, Abs. Ethanol, reflux, 6h; vii) PhCNS, Abs. Ethanol, reflux, 10h; viii) Substituted benzaldehydes, Abs. Ethanol, Glacial acetic acid, reflux, 10h; ix) DMF-DMA, Xylene, piperidine, reflux, 2h.

Scheme 2. Synthesis of derivatives **5-11**, **12a-c** and **13**.

13 was synthesized by reaction of **7** with DMF-DMA. Structures of all derivatives were supported by spectral and elemental analyses.

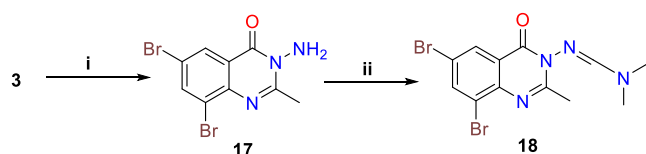
On the other hand, synthesis of compounds **15** and **16a-f** is displayed in **Scheme 3**. First off, a mixture of intermediate **4**, DMF-DMA and piperidine were refluxed in xylene to yield the dimethylaminovinyl compound **14**. Afterwards, compound **14** was converted to **15** using hydrazine hydrate. Arylamino vinyl derivatives **16a-f** were obtained by refluxing compound **14** with the appropriate arylamine in ethanol. Structures of all derivatives were confirmed on basis of spectral and elemental analyses.

Finally, **Scheme 3** shows the synthesis of derivatives **17** and **18** where **17** was obtained by reflux of the benzoxazine **3** with hydrazine hydrate in absolute ethanol. Then, the formamidine derivative **18** was synthesized by reaction of compound **17** with DMF-DMA in the presence of piperidine. Validity of reaction of DMF-DMA solely with the 3-amino of **17** without involvement of the 2-methyl group was affirmed by acquisition of an X-ray crystal of **18** (data provided in the supplementary material). Structures of the synthesized compounds were confirmed by spectral and elemental analyses.



Reagents and conditions: i) DMF-DMA, xylene, piperidine, reflux, 2h; ii) 99% NH₂NH₂, Abs. Ethanol, reflux, 4h; iii) appropriate aromatic amine derivative, Abs. Ethanol, reflux, 4h.

Scheme 3. Synthesis of derivatives **14**, **15** and **16a-f**.



Reagents and conditions: i) 99% NH₂NH₂, Abs. Ethanol, reflux, 12h; ii) DMF-DMA, xylene, piperidine, reflux, 2h

Scheme 4. Synthesis of derivatives **17** and **18**.

2.2. Biology

2.2.1. Cytotoxic activity

2.2.1.1. SRB assay. All twenty-two synthesized compounds were tested for their cytotoxic activity against MCF-7 breast cancer cell line and lung cancer cell line A-549 using SRB assay (Table 1). The synthesized quinazolin-4-ones were more potent on the MCF-7 cells where they showed IC₅₀s in the low to submicromolar range

Table 1

IC₅₀ of the synthesized derivatives against breast cancer cell line MCF-7 and lung cancer cell line A-549 cell lines.

Compd. #	MCF-7 (μM)	A-549 (μM)
5a	≥100	≥100
5b	0.64	12.54
5c	0.12	≥100
7	0.15	≥100
8	40	48.62
9	1	≥100
10	0.58	≥100
11	0.44	26.48
12a	≥100	17.91
12b	20	20.41
12c	40	≥100
13	0.78	61.27
14	0.58	≥100
15	1.7	20.05
16a	2.8	≥100
16b	8	≥100
16c	≥100	67.53
16d	0.63	77.6
16e	1	≥100
16f	70	40.07
17	0.06	≥100
18	≥100	≥100
Doxorubicin	0.06	0.13
5-Fluorouracil	2.13	2.36

while displaying higher micromolar values against the A-549 cell line. Moreover, three compounds (**5a**, **12a** and **18**) were shown to be inactive towards the MCF-7 cells at the experimental threshold in this work with IC₅₀ > 100 μM. In case of A-549 cell lines, nine compounds (**5a**, **5c**, **7**, **9**, **10**, **12c**, **14**, **16a**, **16b**, **16e**, **17** and **18**) have crossed the cutoff value determined for the compounds' activity (>100 μM). Moreover, it was found that compound **17** was the most active against MCF-7 cell lines and **5b** was the most potent compound against both A-549 and (IC₅₀ values of 0.06 μM and 12.54 μM, respectively). Activities were compared to doxorubicin and 5-flourouracil as reference standard drugs.

2.2.1.1.1. SAR findings from in vitro cytotoxicity assay results against MCF-7 cell line. In the acetanilide series **5a-c**, **5a** was not potent (IC₅₀ ≥ 100 μM), however, para substitution on the phenyl ring profoundly improved the activity to the submicromolar range for both compounds **5b** and **5c** (0.64 and 0.12 μM, respectively) with more favoring towards an electron-withdrawing group at para position rather an electron-donating one.

Replacing the phenyl group of **5a** by an aliphatic NH₂ introduced the active compound **7** with IC₅₀ of 0.15 μM indicating that small groups at this position may be in favor towards the activity. Upon comparison of derivative **7** with its bioisosteres compounds **8**, **9** and **10** it was observed that the activity was lowered indicating the importance of the free aliphatic hydrazide to the activity. In compounds **9** and **10**, the presence of a H bond acceptor at position 5 of the pyrazole ring has managed to shift the activity to ≤1 μM when compared with compound **8** of IC₅₀ value of 40 μM.

Upon the reaction of compound **7** with either phenylisothiocyanate to give compound **11** or with different aldehydes to provide the corresponding Schiff's bases **12a-c**, the activity of compound **7** declined with better value in case of compound **11** (0.44 μM) rather than much higher values ≥ 20 μM for the Schiff's bases **12a-c**. Finally, compound **13** which is the dimethylformohydrazonamide of compound **7** has shown IC₅₀ of 0.78 μM that is still a less favorable value than that of compound **7**.

In conclusion, upon comparing the activity of compound **7** with all its derivative (**8**, **9**, **10**, **11**, **12a-c** and **13**) it is clear the activity declined where IC₅₀ fell in the range of 0.44 to ≥ 100 μM when compared to **7** (IC₅₀ = 0.15 μM). It seems that the free hydrazide group at position **3** of the quinazoline ring is favorable for the activity of the scaffold and any substitution has a negative effect on its activity.

Compounds **14**, **15** and **16a-f**, helps in the demonstration of the effect of changing the substituents at position **2**. Compound **14** the main precursor for this series has shown IC₅₀ value of 0.58 μM. All the changes in this moiety has decreased the activity significantly

to fall between 0.63 and 70 μM . Finally, the 3-amino quinazolin-4-one **17** was found to be the most active derivative with $\text{IC}_{50} = 0.06 \mu\text{M}$ (same as doxorubicin). However, replacing the free amino in compound **17** with formamidine group in compound **18** has abolished the activity.

2.2.1.1.2. SAR findings from in vitro cytotoxicity assay results against A-549 cell line. In the acetanilide series **5a-c**, **5b** was the only active compound ($\text{IC}_{50} = 12.54 \mu\text{M}$) which may point out the role of addition of an electron-withdrawing group at the para position of the phenyl ring. Among the derivatives of compound **7**, only **8**, **11**, **12a**, **12b** and **13**. It is clear the inclusion of the hydrazide in a pyrazole ring (compound **8**) enhances the activity when compared to free hydrazide (compound **7**). It is also essential for the ring to be substituted with an electron donating group (compound **8**) rather than an electron withdrawing one (compounds **9** and **10**).

In case of the hydrazide compound **7** and derivatives obtained from it, while compound **7** showed no cytotoxic activity ($\text{IC}_{50} \geq 100 \mu\text{M}$), variable behaviors were observed for its derivatives where some showed enhanced activity where others were still inactive. With regards to the bioisosteric pyrazole derivatives **8** and **9**, compound **8** showed moderate activity with an ($\text{IC}_{50} = 48.6 \mu\text{M}$) which is better than compound **9** which showed no activity ($\text{IC}_{50} \geq 100 \mu\text{M}$). The previous observation may possibly be attributed to the lipophilicity of the methyl group in compound **8** which enhance its cytotoxic activity as compared to the hydrophilic amino group of compound **9** which abolishes the cytotoxic activity. However, it was found the replacement of the pyrazolidine ring in compound **9** with an oxadiazole as in derivative **10**, led also to putting an end to the cytotoxicity ($\text{IC}_{50} \geq 100 \mu\text{M}$).

Relating to the cytotoxic activity of the derivatives **11** & **12a-c** coming from the inactive hydrazide compound **7** ($\text{IC}_{50} \geq 100 \mu\text{M}$), great improvement in the cytotoxicity against the lung cancer cell line A-549 results was observed (IC_{50} range of 17.91–26.84 μM).

Schiff's bases of compounds **12a-c** showed different activity. The best activity in this series was elicited by the parent derivative **12a** which has no substituents on the phenyl ring, where it showed relatively higher activity compared to the other members of this series with IC_{50} of 17.91 μM . On the other hand, the para methoxy derivative **12b** showed a lowered activity having only moderate cytotoxicity (IC_{50} of 40 μM). Moreover, **12c** with an electron withdrawing para chloro substitution was found to have no potency with $\text{IC}_{50} \geq 100 \mu\text{M}$. This indicates that the presence of any substituent in the para position drops off the activity with the electron-donating groups being less favorable than the electron-withdrawing ones. Although compound **14** was inactive, its derivatives **15** has shown IC_{50} of 20.05 μM while **16e** ($\text{IC}_{50} = 7.07 \mu\text{M}$) is considered the most active compound against the A-549 cell lines.

Moreover, the series of compounds **16a-f** showed different activities. The parent unsubstituted derivative **16a** was considered inactive and the *p*-methyl substituent **16b** behaved similarly. The respective *p*-methoxy and the *p*-dimethylamino analogs **16c** and **16d** had slightly increased the cytotoxicity activity with IC_{50} values of 67.53 μM and 77.6 μM respectively. Finally, for this series, the *p*-chlorophenyl derivative **16e** and the compound with a pyridinyl ring in place of the phenyl **16f** gave no activity which indicates that substitution with a lipophilic group or bioisosteric replacement of the phenyl ring demolished the cytotoxic activity.

2.2.1.1.3. Cytotoxic effect of 17 on MDA-MB-231 and MCF10-A. The cytotoxicity of **17** on the triple negative breast cancer cell line MDA-MB-231 was also tested and the IC_{50} was found to be 0.16 nM. Additionally, **17** was tested against the normal breast cell line MCF-10A where it demonstrated a very weak cytotoxic effect ($\text{IC}_{50} = 0.27 \text{ nM}$). These results show that **17** has high selectivity

towards MCF-7 breast cancer cell line being 2.66 folds more cytotoxic when compared to MDA-MB-231. Also, **17** is comparatively safe on normal breast cells being 4.5 folds less cytotoxic.

2.2.2. Investigation of apoptosis against MCF-7

2.2.2.1. Annexin V/PI staining and cell cycle analysis. MCF-7 breast cancer cells were treated with compound **17** for 48 h for investigating its apoptotic activity through cell cycle analysis investigation. Compound **17** significantly increased apoptotic cell death with 25.43-fold (36.11% versus 1.42% for the control). It encouraged the early and late apoptotic, and necrotic cell death by 6.51%, 7.42%, and 22.18% respectively as seen in Fig. 2.

Moreover, DNA flow cytometry for analysis of the cell cycle kinetics was performed in MCF-7 cancer cells to determine the cell population at each phase. As seen in Fig. 3, treatment with **17** significantly increased cell population at the pre-G1 cell cycle phase (36.11% versus 1.24% for the control) and the cell population in the G1 phase (58.31% compared to 44.16% for control). However, it decreased the cell population in both phases G2/M phase (5.45% reduction compared to 8.96% for control) and S phase (36.24% reduction compared to 46.88% for control). Thus, it can be concluded that treatment with **17** induced pre-G1 and G1-phase cell cycle arrest and inhibited the progression of MCF-7 cancer cells.

2.2.2.2. Real time-polymerase chain reaction for the selected genes.

For further investigation of the apoptotic pathway in MCF-7-treated cell with the test compound **17**, RT-PCR reaction was carried out to follow the relative expression of apoptosis-related genes including proapoptotic genes; P53, PUMA, Bax, caspases 3, 8 and 9 and the anti-apoptotic gene Bcl2. As seen in Fig. 4, compound **17** treatment increased the gene expression level of P53 with 9.98-fold, Bax with 5.32-fold, PUMA with 8.11-fold, caspases 3, 8 and 9 with 9.11, 3.14 and 5.44-fold, respectively. On the other hand, it decreased the anti-apoptotic gene Bcl2 with 0.41-fold.

These results are in harmony with previous literature proving the apoptotic behavior through upregulation of proapoptotic and downregulation of antiapoptotic genes. In effect, it can be inferred that both the intrinsic and extrinsic apoptotic pathways were activated.

2.2.3. Investigation of apoptosis against MDA-MB-231

2.2.3.1. Annexin V/PI staining and cell cycle analysis. Compound **17** treated MDA-MB-231 breast cancer cells for 48 h were subjected to cell cycle analysis to determine **17**'s apoptotic effect. Compound **17** significantly increased apoptotic cell death by inducing early and late apoptotic, and necrotic cell death by 2.33%, 14.76% and 11.52%, respectively as shown in Fig. 5.

Additionally, Fig. 6 demonstrates the DNA flow cytometric analysis of the cell cycle kinetics in MDA-MB-231 cancer cells treated with **17**. Results show that treatment significantly increased cell population at the pre-G1 cell cycle phase (28.61% versus 2.19% for the control) and the cell population in the S phase (47.51% compared to 39.84% for control). However, it decreased the cell population in both phases G2/M phase (6.2% compared to 8.8% for control) and G0-G1 phase (46.29% compared to 51.36% for control). Thus, it can be concluded that treatment with **17** induced pre-G1 and S-phase cell cycle arrest and inhibited the progression of MDA-MB-231 cancer cells.

2.2.4. In vivo effect of 17 in a breast cancer solid tumor animal model

2.2.4.1. Antitumor potential on solid carcinoma cells. To evaluate the anti-cancer activity of compound **17** on the cell growth of solid Ehrlich carcinoma (SEC) cells, tumor mice were treated with compound **17** day after day, starting from day 10 following

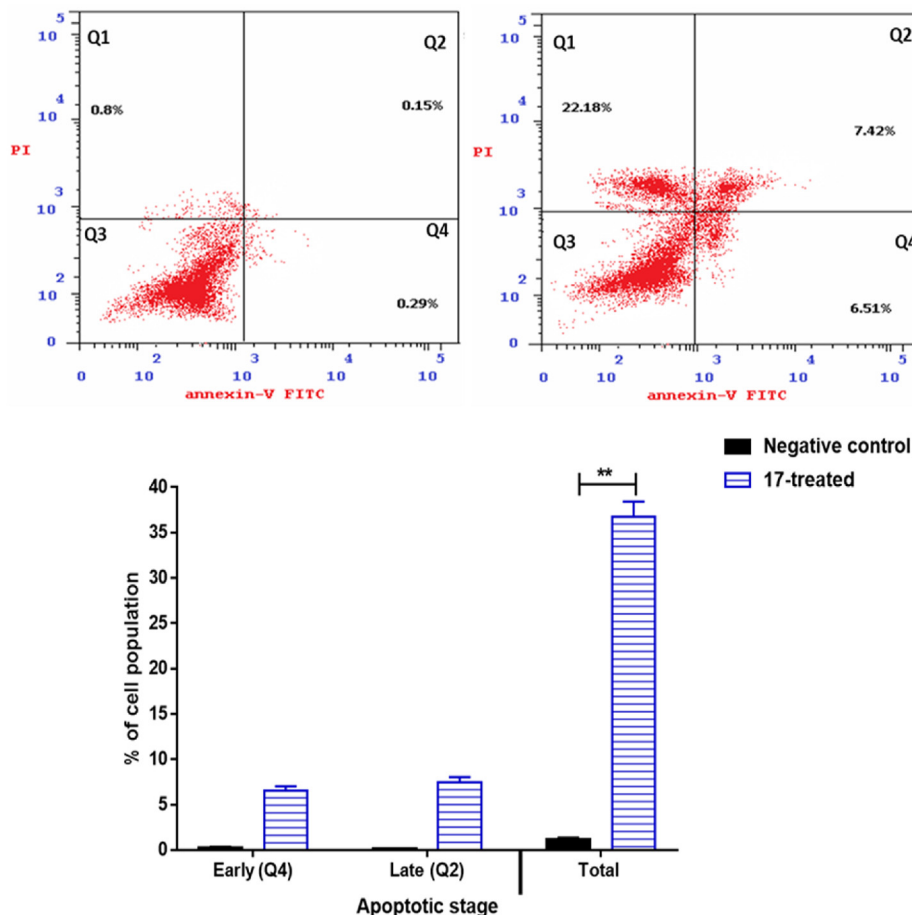


Fig. 2. Cryptographs of annexin-V/Propidium Iodide staining of **Upper left panel:** untreated and **upper right panel:** treated MCF-7 cells with compound **17** ($IC_{50} = 0.06 \mu\text{M}$, 48h). "Q1 (necrotic, AV-/PI+), Q2 (late apoptotic cells, AV+/PI+), Q3 (normal cells, AV-/PI-), Q4 (early apoptotic cells, AV+/PI-), and **lower panel:** Bar-representation of the percentage of cell population in early and late apoptotic cell death. $**P \leq 0.001$ is significantly different to control.

inoculation of tumor cells with a total of seven doses. At the end of the experiment, tumor was excised where the weight and volume of the tumor mass were measured. As seen in Fig. 7, compound **17** treatment significantly decreased the weight of tumor mass from 170 mg in the positive control mice to 65.87 mg being more effective than 5-FU (70.67 mg). Additionally, Compound **17** significantly decreased the tumor volume from 35.2 mm^3 in the positive control mice to 16.7 mm^3 being also better than 5-FU (20 mm^3). In conclusion, compound **17**-treatments significantly inhibited the tumor progression by 52.56% compared to the 43.18% progression inhibition elicited by 5-FU. The results highlighted the promising chemotherapeutic anticancer activity of compound **17**.

Also, the change of the biochemical and hematological parameters upon treatment with **17** was assessed. As seen in Table 2, the SEC control shows elevated levels of serum ALT and AST when compared to a normal group. This observation is an indicative sign of the cancer induced hepatocellular damage. In case of treatment with compound **17**, a significant decline in the serum ALT and AST by 68.57% and 63.37% has been noticed. On the other hand, that decline has been detected to be 69.107% for ALT and 66.88%, for AST for those animals treated with 5-FU when compared to the values of tumor-bearing untreated mice (Table 2). In addition, the serum total protein and albumin levels were higher in tumor bearing-mice than those treated with compound **17** by 148%, and 105.9%, respectively compared to 146.24%, and 103.87%, respectively for 5-FU treated ones.

Additionally, compound **17** treatment has also changed the hematological parameters of SEC-bearing mice are also shown in Table 2. CBC parameters are already changed in SEC mice when compared to normal ones due to the propagating tumor. It was obvious that treatment with compound **17** has led to an increase in the hemoglobin, and RBC's count by 119.37%, and 129.62%, respectively. Treatment with 5-FU has improved the hemoglobin and REBCs count by 116.09% and 126.98%, respectively compared to the values of the untreated tumor-bearing mice. Moreover, treatment with **17** reduced the elevated WBC's in the SEC group count by 80.71%.

It is clear that treatment with compound **17** has multiple effects as it can ameliorate both hematological and biochemical damage caused by the cancer. Therefore, the compound can be promoted for as an interesting analogue with good chemotherapeutic potential and safe treatment outcomes.

2.2.4.2. Histopathological examination for liver tissues. The effect of compound **17** on the liver tissues of SEC mice was evaluated. In normal cells, a regular architecture of the hepatic lobule is maintained where the central vein is surrounded by cords of hepatocytes. Between the strands of hepatocytes, the narrow blood sinusoids are often seen. In SEC-bearing mice there is an observable hydropic degeneration in the hepatocytes where the cell boundaries are lost and ballooning degeneration occur. Some hepatocytes have also shown nuclear pyknosis and karyolysis (Fig. 8). Upon

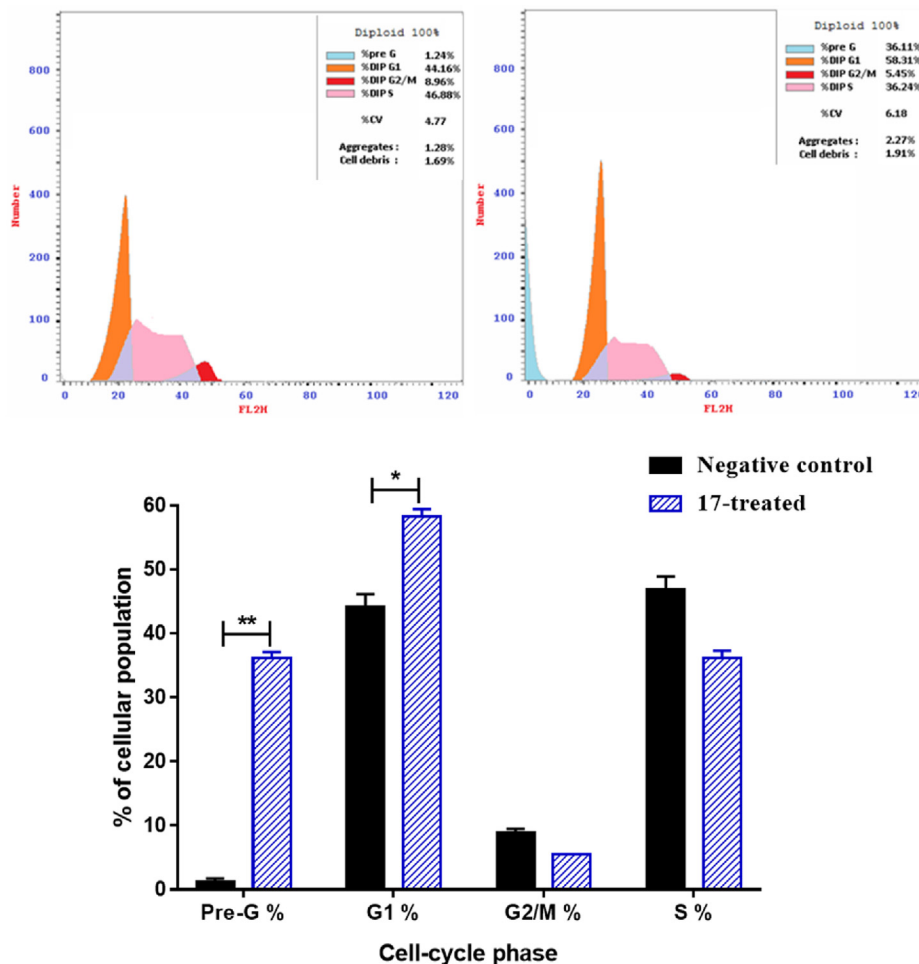


Fig. 3. Histograms DNA content-flow cytometry aided cell cycle analysis of upper left panel: untreated and upper right panel: Treated MCF-7 cells with compound 17 (IC₅₀ = 0.06 μM, 48h), and lower panel: Bar-representation of the percentage of cell population at each cell cycle. Data illustrated is the average of 3 independent experimental runs. **P ≤ 0.001 and *P ≤ 0.05 are significantly different to control.

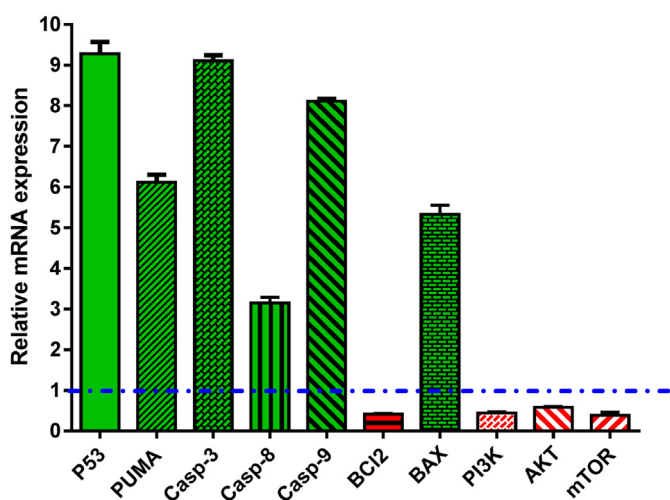


Fig. 4. Gene expression results for the apoptosis-related genes in MCF-7 cells treated with compound 17. Values are expressed as Mean ± SD for 3 independent experimental runs. Dashed horizontal line represents the control (Fold change = 1).

treatment with compound 17, the hepatic lobes in SEC mice have started to regain its original form and looked more like the normal cells. That effect is even better than that found in SEC mice treated

with 5-FU group that still showed hydropic degeneration of the hepatocytes along with nuclear pyknosis and karyolysis. Few hepatocytes showing hydropic degeneration and the activated Kupffer cells were observed.

2.2.5. Effect of treatment by 17 on autophagy

2.2.5.1. Autophagy assessment by acridine orange lysosomal stain. Herein, MCF-7 cells treated with compound 17 (IC₅₀ = 0.06 μM, 48 h) were further inspected for the effect on autophagy using acridine orange lysosomal stain coupled with flow cytometric analysis. Results showed that treatment by compound 17 induced significant reduction in autophagic cell death (9828 cells, average of three independent runs), compared to 11,240 for untreated control cells (P ≤ 0.01) (Fig. 9 displays result of one out of three runs, data of the other two runs are in the supplementary sections). This observation deemed promising as treatment with 17 counteracted autophagy that is usually correlated with enhanced drug resistance and poor prognosis. This is also in line with previous reports that induction of autophagy delays apoptotic cell death [41], thus, it can be inferred that inhibition of autophagy gave way for apoptosis to take place as perceived in the apoptosis study.

These findings combined with the results from cytotoxicity and cell cycle analysis directed us to further investigate the effect of 17 on EGFR, the upstream regulator of autophagy, as detailed in the following sections.

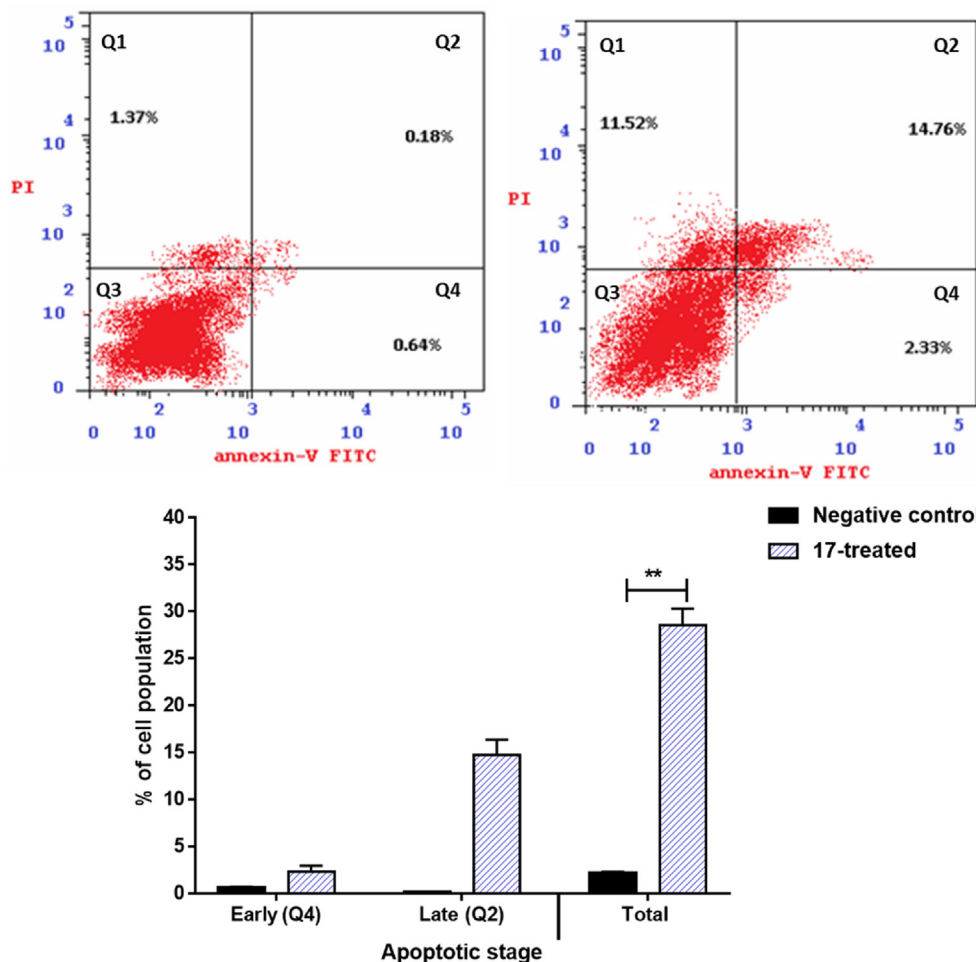


Fig. 5. Cryptographs of annexin-V/Propidium Iodide staining of **upper left panel:** untreated and **upper right panel:** treated MDA-MB-231 cells with compound **17** ($IC_{50} = 0.06 \mu M$, 48h). "Q1 (necrotic, AV-/PI+), Q2 (late apoptotic cells, AV+/PI+), Q3 (normal cells, AV-/PI-), Q4 (early apoptotic cells, AV+/PI-); and **lower panel:** Bar-representation of the percentage of cell population in early and late apoptotic cell death. ****P** ≤ 0.001 is significantly different to control.

2.2.5.2. Effect on EGFR and correlation with autophagy

2.2.5.2.1. Immunohistochemistry of EGFR in vivo expression.

Stimulated by the autophagy assay finding it deemed of interest to investigate the nexus between the autophagy inhibition and EGFR expression as one of the key regulators of autophagy. Thus, solid tumors excised from tumor mice treated as previously described with compound **17** were processed for IHC staining to investigate the expression level of EGFR in these tumor tissues. Results shown in Fig. 10 demonstrated that mice with induced SEC but not subjected to treatment have dark membranous stain reflecting high expression of EGFR. On the contrary, cancer tissues coming from **17** treated cells exhibited much less staining indicating the lower expression of EGFR and thus highlighting the role of compound **17** in downregulation of EGFR in the cancer cells.

2.2.5.3. Effect on PI3K, AKT and PI3K, the downstream effectors of EGFR.

To further explore the correlation between the EGFR lowered expression and the autophagy inhibition, the downstream effectors, PI3K, AKT and mTOR, of the upstream regulator EGFR were investigated using RT-PCR (Fig. 4). Experimental results revealed that genes of the EGFR downstream effectors PI3K, AKT, mTOR were significantly downregulated by 0.44, 0.58 and 0.38-fold, respectively upon treatment of MCF-7 cancer cells with **17**. This observation complies with several other studies that interrelated the EGFR inhibition pathway and EGFR-dependent signaling pathways, especially the PI3K/AKT/mTOR pathway in solid tumor, with

autophagy inhibition as a mechanism towards cancer cell death [42–44].

2.2.5.3.1. Direct effect of 17 on EGFR autophosphorylation and its inhibition in vitro. As it has been well reported that some quinazolin-4-one derivatives elicit part of their cytotoxic action by acting as EGFR inhibitors [45,46], we wanted to test the effect of **17** on EGFR autophosphorylation and determine its IC_{50} in comparison with the well-known EGFR inhibitor erlotinib. Compound **17** has shown significant increase in autophosphorylation percentage inhibition (84.56%) exceeding that of the reference erlotinib (80%) at 10 μM concentration for. Additionally, **17** was more potent as an EGFR inhibitor than erlotinib (IC_{50} s = 0.072 and 0.087 μM , respectively) (Table 3). Collectively it can be inferred that the antitumor effect of quinazolin-4-one **17** is not only driven by reduced autophagy but also by the under-expression and inhibition of the upstream autophagy regulator EGFR as well.

In effect, the obtained results reflect that the mechanism of drug cytotoxicity is pleiotropic being mediated by apoptosis induction, autophagy reduction and EGFR lowered expression as well as EGFR inhibition.

2.3. Molecular docking

Finally, to elucidate the plausible mechanism of binding of **17** to EGFR in comparison to Erlotinib as standard EGFR inhibitor, molecular docking study towards was carried against EGFR protein

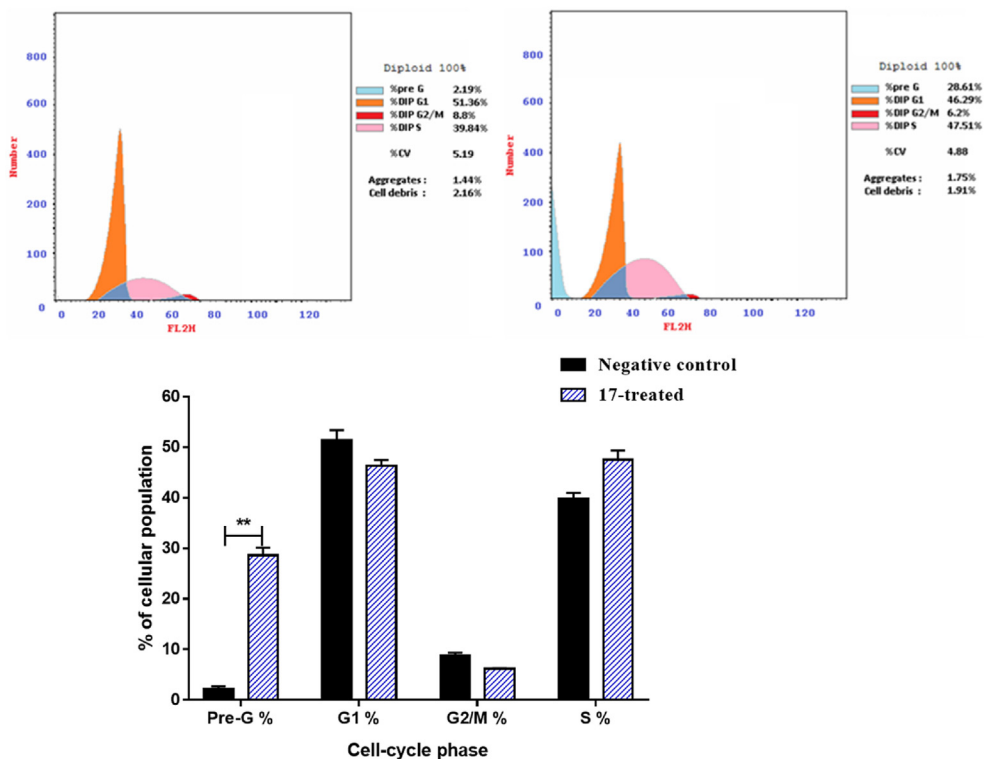


Fig. 6. Histograms of DNA content-flow cytometry aided cell cycle analysis of **upper left panel:** untreated and **upper right panel:** Treated MDA-MB-231 cells with compound **17** ($IC_{50} = 0.06 \mu M$, 48h); and **lower panel:** Bar-representation of the percentage of cell population at each cell cycle. Data illustrated is the average of 3 independent experimental runs. ** $P \leq 0.001$ is significantly different to control.

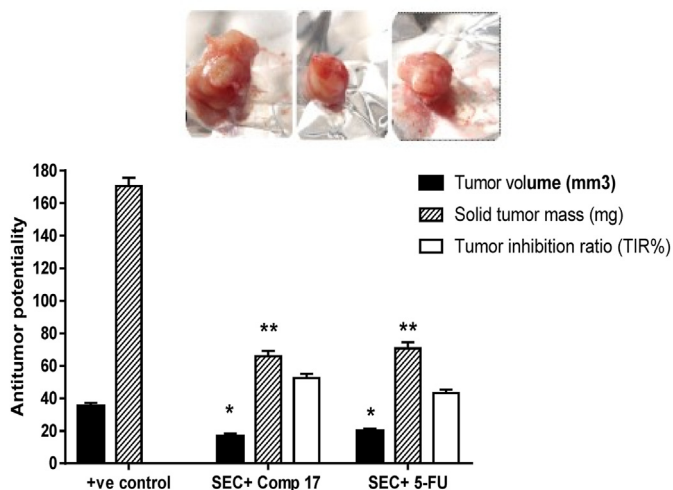


Fig. 7. Compound **17** treatment in solid Ehrlich carcinoma SEC-bearing mice model including tumor mass, volume, tumor inhibition ratio (TIR %). Values are expressed as mean \pm SEM values of mice in each group ($n = 5$). ** $P \leq 0.001$ and * $P \leq 0.05$ are significant different to the positive control using an unpaired *t*-test using GraphPad prism.

(PDB = 1M17) using MOE version 2019.01. As illustrated in (Fig. 11), compound **17** had a good recognition to the ATP binding site of EGFR in a similar fashion to Erlotinib. While Erlotinib displayed a binding score of -7.57 kcal/mol, **17** had a -5.23 kcal/mol, binding score. Also, compound **17** formed the same binding interactions as Erlotinib, which also formed one HB with Met769 as HB-acceptor through the quinazoline oxygen in addition to a pi-H interaction with Val702. It is well recognized that docking scores do not

precisely reflect the actual ligand enzyme inhibition capacity so S scores are only displayed here for the sake of approximate binding energetics calculation.

Overall taken together, the combined results EGFR related studies introduce compound **17** as a promising EGFR potent inhibitor with simple structure through three integrated approaches *in vitro*, *in vivo* and *in silico*.

3. Conclusion

In the current study, a series of quinazolin-4-one derivatives has been synthesized and studied as potential anticancer agents. The developed compounds were tested against two cancer cell lines namely MCF-7 and A-549 where all of them showed better activity towards the MCF-7 breast cancer cell lines with IC_{50} s values in the low to sub-micromolar range. Compound **17**, the most active in this study, exhibited an IC_{50} of $0.06 \mu M$ being equipotent to doxorubicin and more potent than 5-FU. Investigation into the mechanism of action of **17**, as a representative of this class, has revealed its capacity to induce intrinsic and extrinsic apoptosis, effect cell cycle arrest and reduce autophagy. *In vivo*, it was able to reduce tumor mass and volume while maintaining normal biochemical and hematological parameters and a near normal liver histopathology with a better outcome than 5-FU. Additionally, **17** was able to reduce the EGFR expression levels in tumors of treated mice along with demonstrating a capacity to inhibit the enzymatic activity of EGFR compared to that of erlotinib. Also, the downstream effectors of EGFR, viz. PI3K, AKT and mTOR, were downregulated upon treatment of MCF-7 cells with **17**. Docking of **17** with EGFR demonstrated its ability to bind with key active site amino acids like erlotinib. In conclusion, this study discloses a new class of potent anticancer agents that have a pleotropic mode of action that

Table (2)
Biochemical and hematological parameters in the tested groups.

Parameter/Treatment	ALT (U/L)	AST (U/L)	Total Protein (g/dL)	Albumin (g/dL)	Hb (g/dL)	RBCs count (× 106/μL)	WBCs count (× 103/μL)
Normal control	40.3 ± 3.5	47.4 ± 2.8	7.6 ± 0.4	6.4 ± 0.4	8.02 ± 0.4	5.04 ± 0.76	3.69 ± 0.53
SEC control	56 ± 2.7	59.8 ± 3.7	5.06 ± 0.4	3.87 ± 0.7	6.4 ± 0.6	3.78 ± 0.42	5.34 ± 0.65
SEC + 17 (5 mg/kg BW)	38.4* ± 9.1	37.9* ± 8.4	7.5* ± 0.2	4.1 ± 0.2	7.64 ± 0.5	4.9 ± 0.58	4.31 ± 0.68
SEC + 5-FU (5 mg/kg BW)	38.7* ± 3.5	40* ± 4.6	7.4* ± 0.4	4.02 ± 0.3	7.43 ± 0.6	4.8 ± 0.43	4.54 ± 0.98

- Values are expressed as Mean ± SEM of 3 independent experiments.

*Significant difference between treated groups and SEC control using unpaired t-test ($P \leq 0.05$) using the GraphPad prism7).

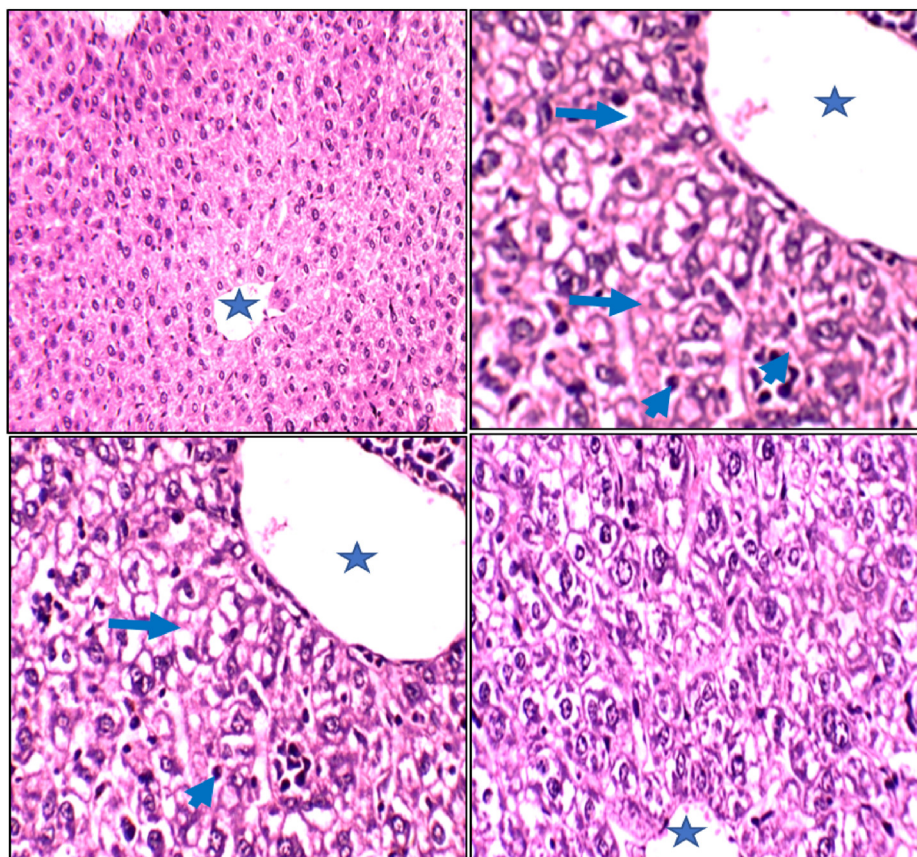


Fig. 8. Upper left panel: Normal control group. The central vein (asterisk) surrounded by cords of hepatocytes. Upper right panel: SEC untreated control group mice, nuclear pyknosis (arrowheads) and karyolysis (arrows); lower left panel: SEC mice treated with compound 17; lower right panel: SEC mice treated with 5-FU group, nuclear pyknosis (arrowheads) and karyolysis (arrows). (H&E stain: upper left panel magnification × 200; other panels magnification × 400).

can serve as leads for further optimization and future drug discovery of small molecules related to this chemotype.

4. Experimental

4.1. Chemistry

Melting points were recorded on Stuart Scientific apparatus and were uncorrected. FT-IR spectra were recorded on a Perkin–Elmer spectrophotometer. ^1H NMR and ^{13}C NMR spectra were obtained using Varian Mercury-300 NMR Spectrometer or Bruker Avance 400 MHz NMR Spectrometer using TMS as an internal standard. Elemental analyses were carried out at the Microanalytical center, Faculty of Pharmacy, Al-Azhar University, Egypt and are within $\pm 0.4\%$ of the calculated values. Mass spectra were carried out at the micro analytical unit, Faculty of Science, Cairo University. All chemical and solvents were purchased from Sigma Aldrich and used as provided. Compounds (**2–4**, **6** and **7**) were synthesized and confirmed according to the reported data [36,37,47,48].

4.1.1. General procedure of synthesis of 2-(6, 8-dibromo-2-methyl-4-oxoquinazolin-3(4H)-yl)-N-arylacetamide (5a-c)

To a solution of compound **4** (0.32 gm, 1 mmol) in dry acetone (20 mL) was added anhydrous K_2CO_3 (0.276 gm, 2 mmol) and the corresponding substituted 2-chloro-N-phenylacetamide (1 mmol). The reaction mixture was refluxed overnight. Upon reaction completion, the solvent was evaporated under reduced pressure followed by recrystallization of the residue to obtain the corresponding derivatives **5a-c**.

4.1.1.1. 2-(6,8-Dibromo-2-methyl-4-oxoquinazolin-3(4H)-yl)-N-phenylacetamide (5a). White powder, Yield, 88%, m.p. > 300 °C. IR (cm^{-1}): 3320 (NH), 3141 (CH arom.), 2956–2933 (CH aliph.), 1691 (C=O), 1656 (C=O). ^1H NMR (300 MHz, DMSO- d_6) ppm: δ 2.6 (s, 3H), 4.98 (s, 2H), 7.05–7.08 (m, 1H), 7.30–7.32 (m, 2H), 7.51 (d, 2H, $J = 7.8$ Hz) 8.1 (s, 1H), 8.3 (s, 1H), 10.46 (s, 1H). MS m/z (%): 453 ($\text{M}^+ + 4$), 451 ($\text{M}^+ + 2$), 449 (M^+). Anal. Calcd. for $\text{C}_{17}\text{H}_{13}\text{Br}_2\text{N}_3\text{O}_2$ (451): C, 45.26; H, 2.90; N, 9.31, Found: C, 45.41; H, 2.97; N, 9.38.

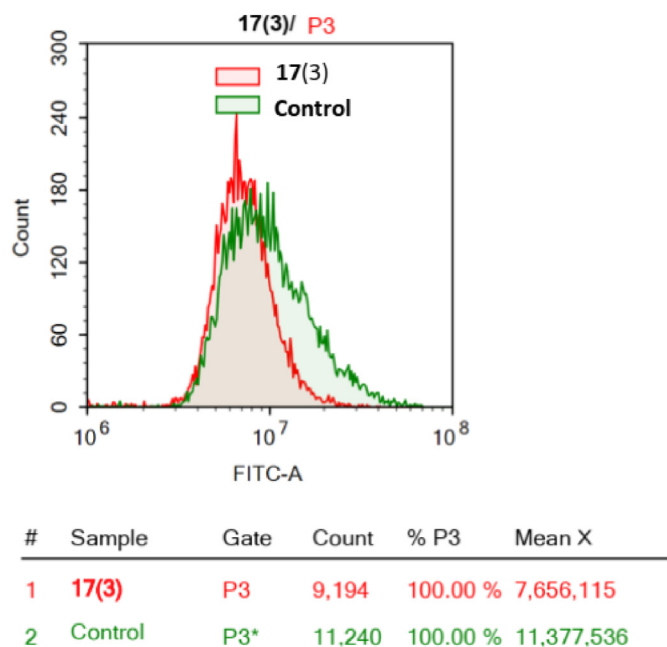


Fig. 9. Autophagic cell death assessment in MCF-7 treated with compound 17 ($IC_{50} = 0.06 \mu M$, 48 h) using the acridine orange lysosomal stain coupled with the flow cytometric analysis. **Green:** Negative control (untreated), **Red:** Compound 17-treated cells (data presented is for one out of three independent runs).

4.1.1.2. 2-(6,8-Dibromo-2-methyl-4-oxoquinazolin-3(4H)-yl)-N-(p-tolyl)acetamide (5b). White powder, Yield, 90%, m.p. > 300 °C. IR (cm^{-1}): 3267 (NH), 3136 (CH arom.), 2962-2923 (CH aliph.), 1689 (C=O), 1654 (C=O). 1H NMR (300 MHz, DMSO- d_6): δ 2.25 (s, 3H), 2.49 (s, 3H), 4.95 (s, 2H), 7.12 (d, 2H, $J = 6$ Hz), 7.45 (d, 2H, $J = 6$ Hz), 8.1 (s, 1H), 8.3 (s, 1H), 10.3 (s, 1H). MS m/z : 467 ($M^+ + 4$), 465 ($M^+ + 2$), 463 (M^+). Anal. Calcd. of $C_{18}H_{15}Br_2N_3O_2$ (465): C, 46.48;

H, 3.25; N, 9.03, Found: C, 46.76; H, 3.31; N, 9.18.

4.1.1.3. N-(4-Chlorophenyl)-2-(6,8-dibromo-2-methyl-4-oxoquinazolin-3(4H)-yl)acetamide (5c). White powder, Yield, 89%, m.p. > 300 °C, IR (cm^{-1}): 3286 (NH), 3061 (CH arom.), 2937-2850 (CH aliph.), 1683 (C=O), 1651 (C=O). 1H NMR (300 MHz, DMSO- d_6): δ 1.54 (s, 3H), 4.88 (s, 2H), 7.47 (d, 2H, $J = 8$ Hz), 7.66 (d, 2H, $J = 8$ Hz), 8.17 (s, 1H), 8.38 (s, 1H), 10.27 (s, 1H). Anal. Calcd. for $C_{17}H_{12}Br_2ClN_3O_2$ (486): C, 42.05; H, 2.49; N, 8.65, Found: C, 42.21; H, 2.56; N, 8.82.

4.1.2. 6,8-Dibromo-3-(2-(2,3-dihydro-3-hydroxy-5-methylpyrazol-1-yl)-2-oxoethyl)-2-methylquinazolin-4(3H)-one (8)

A mixture of compound 7 (0.39 gm, 1 mmol) and ethyl acetate (0.13 gm, 1 mmol) was refluxed in ethanol for 6 h, The product was obtained as a white powder; Yield, 80%, m.p. < 300 °C; IR (cm^{-1}): 3064 (CH arom.), 2972 (CH aliph.), 1685, 1668 (C=O), 1H NMR (300 MHz, DMSO- d_6): δ 1.8 (s, 3H), 2.45 (s, 3H), 4.86 (s, 2H), 6.82 (s, 1H), 8.16 (s, 1H), 8.34 (s, 1H), 9.88 (s, 1H); ^{13}C NMR (100 MHz, DMSO- d_6): δ 20.87, 23.62, 45.57, 118.98, 122.63, 123.23, 128.66, 140.18, 144.19, 157.48, 160.10, 165.91, 166.05, 168.57. MS m/z : 457 ($M^+ + 3$), 456 ($M^+ + 2$), peaks for bromine isotope (312, 310), (156, 154), (198, 196), (103, 101). Anal. Calcd. for $C_{15}H_{12}Br_2N_4O_3$ (456): C, 39.50; H, 2.65; N, 12.28, Found: C, 39.66; H, 2.71; N, 12.34.

4.1.3. 6,8-Dibromo-3-(2-(3-hydroxy-5-imino-2H-pyrazol-1(5H)-yl)-2-oxoethyl)-2-methylquinazolin-4(3H)-one (9)

A mixture of compound 7 (0.39 gm, 1 mmol) and ethyl cyanoacetate (0.11 gm, 1 mmol) was refluxed in glacial acetic acid for 6 h. The product was obtained as a white powder; Yield, 85%, m.p. < 300 °C. IR (cm^{-1}): 3588 (NH), 3446 (NH), 3062 (CH arom.), 2972 (CH aliph.), 1683, 1670, 1655 (C=O); 1H NMR (300 MHz, DMSO- d_6): δ 1.85 (s, 3H), 2.56 (s, 1H), 4.85 (s, 2H), 8.15 (s, 1H), 8.29 (s, 1H), 9.88 (s, 1H), 10.24 (s, 1H); MS m/z : 459 ($M^+ + 4$), 457 ($M^+ + 2$), 455 (M^+). Anal. Calcd. for $C_{14}H_{11}Br_2N_5O_3$ (457): C, 36.79; H, 2.43; N, 15.32, Found; C, 36.90; H, 2.51; N, 15.44.

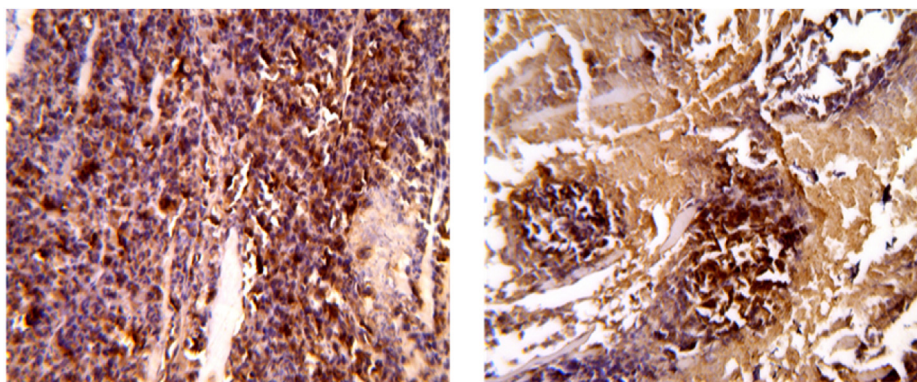


Fig. 10. Immunohistochemical staining for EGFR of solid tumor sections. **Right panel:** Negative control mice-induced SEC; **left panel:** Mice-induced SEC and treated with compound 17 (magnification: $\times 200$).

Table (3)
EGFR autophosphorylation inhibition and IC_{50} of 17.

Cmpds	Autophosphorylation percentage inhibition	EGFR PK inhibition, IC_{50} [μM]
17	84.56 \pm 1.19*	0.072 \pm 0.00574**
Erlotinib	80.05 \pm 1.07	0.087 \pm 0.00621

- values are expressed as mean \pm SD of three independent replicas.

- IC_{50} values were calculated using sigmoidal non-linear regression curve fit of percentage inhibition against five concentrations of each compound.

* $P \leq 0.05$, ** $P \leq 0.001$.

Compd	Binding energy (Kcal/mol)	Ligand-receptor interactions		
		HB interactions	Distance (Å)	Lipophilic interactions
Erlotinib	-7.57	1 HB with Met 769 as the key amino acid of interaction	1.70	Good lipophilic interactions with Met 769, Ala 719, Leu 620, Phe 771, Leu 694, Pro 770, Leu 768, and Leu 764
17	-5.23		1.97	

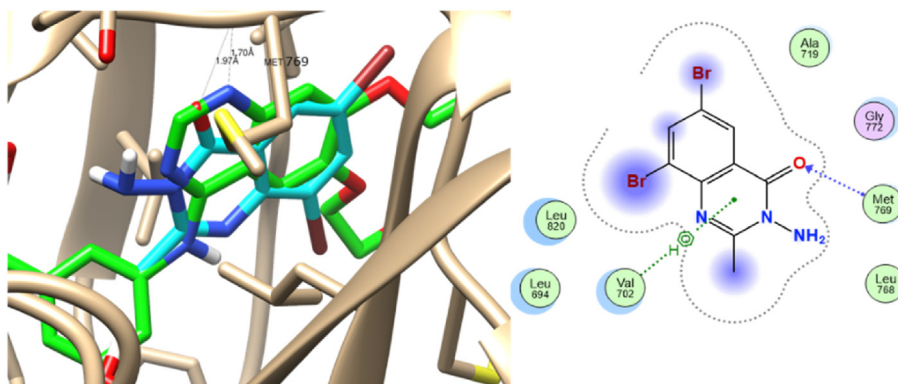


Fig. 11. Ligand-receptor interactions within the ATP binding site of EGFR (PDB = 1M17). **Upper panel:** binding details; **bottom left panel:** 3D representation generated by Chimera of binding disposition of Erlotinib (Cyan) and **17** (Orange) with EGFR; **bottom right panel:** 2D representation of **17** generated by MOE 2019.01.

4.1.4. 6,8-Dibromo-3-(5-mercapto-3-oxo-3H-pyrazol-4-yl)-2-methylquinazolin-4(3H)-one (10)

A mixture of compound **7** (0.39 gm, 1 mmol) and carbon disulfide (0.07 gm, 1 mmol) was refluxed in absolute ethanol for 6 h, Yellowish white powder; m.p. < 300 °C, Yield, 88%; IR (cm⁻¹): 3058 (CH arom.), 2940 (CH aliph), 2361 (SH), 1687 (C=O), 1626 (C=O). ¹H NMR (300 MHz, DMSO-*d*₆): δ 2.38 (s, 3H), 8.14 (d, 1H, Hz = 2.1), 8.28 (d, 1H, Hz = 2.1), 12.57 (s, 1H). ¹³C NMR (100 MHz, DMSO-*d*₆): δ 22.34, 118.37, 123.14, 123.73, 128.16, 139.89, 146.05, 156.67, 160.66. Anal. Calcd. for C₁₂H₆Br₂N₄O₂S (430): C, 33.36; H, 1.87; N, 12.97; Found: C, 33.19; H, 2.23; N, 12.61.

4.1.5. 1-(2-(6,8-Dibromo-2-methyl-4-oxoquinazolin-3(4H)-yl)acetyl)-4-phenylthiosemicarbazide (11)

A mixture of compound **7** (0.39 gm, 1 mmol) and phenylisothiocyanate (0.13 gm, 1 mmol) was refluxed in ethanol for 10 h where the corresponding thiosemicarbazide was obtained and confirmed as reported [40,49].

4.1.6. General procedure for synthesis of Schiff's bases *N'*-Arylidinene-2-(6,8-dibromo-2-methyl-4-oxoquinazolin-3(4H)-yl)acetohydrazide (12a-c)

A mixture of **7** (0.39 gm, 1 mmol) and benzaldehyde derivatives (1 mmol) in absolute ethanol (10 mL) and a few drops of acetic acid was refluxed for 10 h, and the reaction mixture left to cool. The solid was then filtered off, and crystallized from ethanol/acetic acid [40].

4.1.6.1. *N'*-Benzylidene-2-(6,8-dibromo-2-methyl-4-oxoquinazolin-3(4H)-yl)acetohydrazide (12a). White powder, m.p. 263–265 °C, Yield, 80% as reported [38].

4.1.6.2. 2-(6,8-Dibromo-2-methyl-4-oxoquinazolin-3(4H)-yl)-*N'*-(4-methoxybenzylidene)acetohydrazide (12b). White powder; Yield, 77%; m.p. < 300 °C; IR (cm⁻¹): 3203 (NH), 3061 (CH arom.), 2972 (CH aliph.), 1683, 1668 (C=O). ¹H NMR (400 MHz, DMSO-*d*₆): δ 2.50 (s, 3H), 3.81 (s, 3H), 5.30 (s, 2H), 7.01 (dd, 2H, *J* = 4.8, 8.8 Hz), 7.64

(dd, 2H, *J* = 4.8, 8.8 Hz), 8.01 (s, 1H), 8.17 (d, *J* = 2 Hz, 1H), 8.37 (d, *J* = 2 Hz, 1H), 11.75 (s, 1H, NH, -D₂O exchangeable). MS *m/z*: 510 (M⁺ + 4), 508 (M⁺ + 2), 506 (M⁺). Anal. Calcd. for C₁₉H₁₆Br₂N₄O₃ (508): C, 44.91; H, 3.17; N, 11.03, Found: C, 45.1; H, 3.23; N, 11.23.

4.1.6.3. *N'*-(4-Chlorobenzylidene)-2-(6,8-dibromo-2-methyl-4-oxoquinazolin-3(4H)-yl)acetohydrazide (12c). White powder, as reported [50].

4.1.7. 2-(6,8-Dibromo-2-methyl-4-oxoquinazolin-3(4H)-yl)-*N'*-(dimethylamino-methylene)acetohydrazide (13)

A mixture of compound **7** (0.39 gm, 1 mmol) and DMF-DMA (0.12 mL, 1 mmol) was refluxed in xylene for 3 h. The solid obtained was crystallized from ethanol. Yellow powder, Yield, 77%; m.p. 260–262 °C; IR (cm⁻¹): 3226 (NH), 3066 (CH arom.), 2972 (CH aliph.), 1691 (C=O), 1627 (C=O). ¹H NMR (400 MHz, DMSO-*d*₆): δ 2.49 (s, 3H), 2.81 (s, 6H), 4.72 (s, 2H), 5.01 (s, 1H), 8.16 (s, 1H), 8.34 (s, 1H), 10.59 (s, 1H). MS *m/z*: 402 [M⁺ + 4 - N(CH₃)₂], 400 [M⁺ + 2 - N(CH₃)₂], 498 [M⁺ - N(CH₃)₂], peaks for bromine isotopes (323, 321), (239, 237), (210, 208). Anal. Calcd. for C₁₄H₁₅Br₂N₅O₂ (445): C, 37.78; H, 3.40; N, 15.73, Found; C, 37.90; H, 3.54; N, 15.88.

4.1.8. 6,8-Dibromo-2-((*E*)-2-((dimethylamino)vinyl)quinazolin-4(3H)-one (14)

Compound **4** was dissolved in xylene (10 mL), 3 drops of piperidine were added and the mixture was refluxed for 10 min, after which DMF-DMA (1.2 mL, 1 mmol) was added & refluxed for 1 h. The solvent was evaporated and the solid obtained was recrystallized from ethanol as golden yellow powder; Yield, 88%; m.p. 250–252 °C; IR (cm⁻¹): 3171 (NH), 3050 (CH arom.), 2937 (CH aliph.), 1665 (C=O), 1618 (CH=CH). ¹H NMR (400 MHz, DMSO-*d*₆): δ 3.48 (s, 6H), 5.06 (d, 1H, *J* = 11.92 Hz), 7.98 (s, 1H), 8.06 – 8.09 (m, 2H), 8.60 (s, 1H, NH, D₂O-exchangeable). MS *m/z*: 375 (M⁺ + 4), 373 (M⁺ + 2), 371 (M⁺). Anal. Calcd. for C₁₂H₁₁Br₂N₃O (373): C, 38.64; H, 2.97; N, 11.26, Found: C, 38.87; H, 3.01; N, 11.44.

4.1.9. 6,8-Dibromo-2-(2-hydrazinylvinyl)quinazolin-4(3H)-one (15)

A mixture of compound **14** (0.37 gm, 1 mmol) and hydrazine hydrate 99% (0.04 gm, 1 mmol) in absolute ethanol (20 mL) was refluxed for 3 h where the product was then obtained by crystallization from ethanol, Yellow precipitate, m.p. > 300 °C, Yield, 66%, IR (cm⁻¹): 3200 (NH₂), 3132 (NH), 3059 (CH arom.), 2937 (CH aliph.), 1669 (C=O). ¹H NMR (400 MHz, DMSO-*d*₆): δ 4.60 (br s, 2H, NH₂, D₂O-exchangeable), 5.20 (d, 1H, *J* = 8 Hz), 7.68–7.73 (m, 1H), 8.13 (d, 1H, *J* = 2.4 Hz), 8.23 (d, 1H, *J* = 2.4 Hz), 12.15 (s, 1H, NH, D₂O-exchangeable), 12.60 (s, 1H, D₂O-exchangeable). Anal. Calcd. For C₁₀H₈Br₂N₄O (360): C, 33.36; H, 2.24; N, 15.56, Found: C, 33.61; H, 2.32; N, 15.22.

4.1.10. General method for synthesis of 6,8-dibromo-2-((E)-2-(arylamino)vinyl)quinazolin-4(3H)-ones (16a-f)

A mixture of compound **14** (0.37 gm, 1 mmol) and the appropriate aniline (1 mmol) in ethanol was refluxed for 3 h to obtain the compounds (**16a-f**).

4.1.10.1. 6,8-Dibromo-2-(2-(phenylamino)vinyl)quinazolin-4(3H)-one (16a). Yellow powder; Yield, 75%, m.p. > 300 °C; IR (cm⁻¹): 3385 (NH), 3134 (NH), 3037 (CH arom.), 2922 (CH aliph.), 1664 (C=O), 1669 (C=C). ¹H NMR (400 MHz, DMSO-*d*₆): δ 5.20 (d, 1H, *J* = 8.4 Hz), 7.03 (t, 1H, *J* = 8 Hz), 7.30–7.39 (m, 4H), 7.83 (dd, *J* = 8.4, 12.5 Hz, 1H), 8.10 (d, 1H, *J* = 2.2 Hz), 8.32 (d, 1H, *J* = 2.2 Hz), 11.65 (d, 1H, *J* = 12.5 Hz), 12.25 (s, 1H, NH, D₂O-exchangeable). MS *m/z*: 423 (M⁺ + 4), 421 (M⁺ + 2), 419 (M⁺). Anal. Calcd. for C₁₆H₁₁Br₂N₃O (421): C, 45.64; H, 2.63; N, 9.98, Found: C, 45.78; H, 2.68; N, 10.14.

4.1.10.2. 6,8-Dibromo-2-(2-(*p*-tolylamino)vinyl)quinazolin-4(3H)-one (16b). Yellow powder, Yield, 70%, m.p. > 300 °C; IR (cm⁻¹): 3446 (NH), 3132 (NH), 3051 (CH arom.), 2970 (CH aliph.), 1672 (C=O), 1633 (C=C). ¹H NMR (400 MHz, DMSO-*d*₆): δ 2.26 (s, 3H), 5.15 (d, 1H, *J* = 8.4 Hz), 7.15 (d, 2H, *J* = 8.8 Hz), 7.18 (d, 2H, *J* = 8.8 Hz), 7.72 (dd, 1H, *J* = 8.4, 1.5 Hz), 8.07 (d, 1H, *J* = 2 Hz), 8.28 (d, 1H, *J* = 2 Hz), 11.61 (d, 1H, *J* = 12.5 Hz), 12.18 (s, 1H). MS *m/z* (%): 437 (M⁺ + 4), 435 (M⁺ + 2), 433 (M⁺). Anal. Calcd. for C₁₇H₁₃Br₂N₃O (435): C, 46.93; H, 3.01; N, 9.66, Found: C, 47.12; H, 3.05; N, 9.84.

4.1.10.3. 6,8-Dibromo-2-(2-((4-methoxyphenyl)amino)vinyl)quinazolin-4(3H)-one (16c). Yellow powder, Yield, 78%, m.p. > 300 °C. IR (cm⁻¹): 3400 (NH), 3132, 3048 (CH arom.), 2949 (CH aliph.), 1678 (C=O), 1629 (CH=CH). ¹H NMR (400 MHz, DMSO-*d*₆): δ 3.72 (s, 3H), 5.11 (d, 1H, *J* = 8.4 Hz), 6.93 (d, 2H, *J* = 8.8 Hz), 7.23 (d, 2H, *J* = 8.8 Hz), 7.72 (dd, 1H, *J* = 8.4, 12.5 Hz), 8.06 (d, 1H, *J* = 2 Hz), 8.27 (d, 1H, *J* = 2 Hz), 11.63 (d, 1H, *J* = 12.5 Hz), 12.15 (s, 1H). MS *m/z*: 453 (M⁺ + 4), 451 (M⁺ + 2), 499 (M⁺). Anal. Calcd. for C₁₇H₁₃Br₂N₃O₂ (451): C, 45.26; H, 2.9, N, 9.31, Found: C, 45.49; H, 2.9; N, 9.45.

4.1.10.4. 6,8-Dibromo-2-(2-((4-(diethylamino)phenyl)amino)vinyl)quinazolin-4(3H)-one (16d). yellow powder; Yield, 80%, m.p. > 300 °C; IR (cm⁻¹): 3446 (NH), 3421 (NH), 3061 (CH arom.), 2972 (CH aliph.), 1683 (C=O), 1627 (CH=CH). ¹H NMR (300 MHz, DMSO-*d*₆): δ 1.06 (t, 6H, *J* = 6.9 Hz), 3.3 (q, 4H, *J* = 6.9 Hz), 5.06 (d, 1H, *J* = 8.1 Hz), 6.69 (d, 2H, *J* = 8.7 Hz), 7.13 (d, 2H, *J* = 8.7 Hz), 7.68 (dd, 1H, *J* = 8.1, 12.5 Hz), 8.05 (d, 1H, *J* = 2.4 Hz), 8.25 (d, 1H, *J* = 2.4 Hz), 11.68 (d, 1H, *J* = 12.5 Hz, NH, D₂O-exchangeable), 12.1 (s, 1H, NH D₂O-exchangeable). MS *m/z*: 494 (M⁺ + 4), 492 (M⁺ + 2), 490 (M⁺), peaks for bromine isotopes: (449, 447), (238, 236), (195, 193), (93, 91). Anal. Calcd. for C₂₀H₂₀Br₂N₄O (492): C, 48.80; H, 4.10; N, 11.38, Found: C, 49.03; H, 4.17; N, 11.61.

4.1.10.5. 6,8-Dibromo-2-(2-((4-chlorophenyl)amino)vinyl)quinazolin-4(3H)-one (16e). Yellow powder; Yield, 80%; m.p. > 300 °C. IR

(cm⁻¹): 3414, 3132 (NH), 3066 (CH arom.), 2966–2920 (CH aliph.), 1676 (C=O), 1631 (CH=CH). ¹H NMR (300 MHz, DMSO-*d*₆): δ 5.35 (d, 1H, *J* = 8.1 Hz), 7.29–7.22 (m, 4H), 7.80 (dd, 1H, *J* = 8.1, 12.5 Hz), 8.05 (d, 1H, *J* = 2 Hz), 8.21 (d, 1H, *J* = 2 Hz), 11.94 (d, 2H, *J* = 12.5 Hz, 2NH, D₂O-exchangeable). ¹³C NMR (100 MHz, DMSO-*d*₆): δ 29.96, 86.85, 115.49, 116.07, 120.10, 120.57, 128.19, 129.81, 130.64, 138.60, 138.93, 142.32, 143.75, 156.01, 159.28, 172.77. MS *m/z*: 455 (M⁺ + 2), 453 (M⁺). Anal. Calcd. for C₁₆H₁₀Br₂ClN₃O (456): C, 42.19; H, 2.21; N, 9.22, Found: C, 42.38; H, 2.08; N, 9.37.

4.1.10.6. 6,8-Dibromo-2-(2-(pyridin-2-ylamino)vinyl)quinazolin-4(3H)-one (16f). Off white powder; Yield, 77%; m.p. 275 °C, IR (cm⁻¹): 3404, 3346 (NH), 3068 (CH arom.), 2933 (CH aliph.), 1685 (C=O), 1622 (CH=CH). ¹H NMR (400 MHz, DMSO-*d*₆): δ 5.23 (d, 1H, *J* = 8 Hz), 7.89–8.10 (m, 6H), 8.21 (d, 1H, *J* = 2.4 Hz), 11.75 (s, 1H), 12.60 (s, 1H). MS *m/z*: 424 (M⁺ + 4), 423 (M⁺ + 3), 422 (M⁺ + 2), peaks for bromine isotopes: (413, 411), (417, 415), (277, 275), (247, 245), (221, 219), (145, 143). Anal. Calcd. for C₁₅H₁₀Br₂N₄O (422): C, 42.68; H, 2.39; N, 13.27, Found: C, 42.92; H, 2.44; N, 13.43.

4.1.11. 3-Amino-6,8-dibromo-2-methylquinazolin-4(3H)-one (17)

An equimolar mixture of compound **3** (0.319 gm, 1 mmol) and hydrazine hydrate 99% (0.5 mL, 1 mmol) in 20 mL absolute ethanol was refluxed for 12 h. Upon reaction completion, the mixture was concentrated in vacuum where compound **17** was obtained as white crystals upon recrystallization from ethanol and confirmed as reported [51,52].

4.1.12. N'-(6,8-dibromo-2-methyl-4-oxoquinazolin-3(4H)-yl)-N,N-dimethylformamide (18)

Compound **17** (0.33 gm, 1 mmol) and DMF-DMA (1.2 mL, 1 mmol) were refluxed in xylene (10 mL) for 90 min. After cooling and evaporating the solvent, large colourless needle crystals were obtained. Yield, 77%; m.p. 170–172 °C. IR (cm⁻¹): 3056 (CH arom.), 2934 (CH aliph.), 1668 (C=O), 1622 (CH=N). ¹H NMR (300 MHz, DMSO-*d*₆): δ 2.48 (s, 3H), 2.96 (s, 6H), 7.90 (s, 1H), 8.04 (s, 1H), 8.15 (s, 1H). Mass *m/z*: 346 [M⁺ + 4 - N(CH₃)₂], 344 [M⁺ + 2 - N(CH₃)₂], 342 [M⁺ - N(CH₃)₂], peaks for bromine isotopes: (290, 288), (278, 276), (263, 261), (225, 223), (196, 194), (155, 153). Anal. Calcd. for C₁₂H₁₂Br₂N₄O (388): C, 37.14; H, 3.12 N, 14.44, Found: C, 37.39, H, 3.19, N, 14.47.

4.2. Biology

4.2.1. Cytotoxic activity via SRB assay

MCF-7 human tumor cell line, (breast adenocarcinoma) was grown as monolayer and routinely maintained in RPMI-1640 medium supplemented with 5% heat inactivated FBS, 2 mM glutamine and antibiotics (penicillin 100 U/ml, streptomycin 100 µg/ml), at 37 °C in a humidified atmosphere containing 5% CO₂. Exponentially growing cells were obtained by plating 1.5 × 10⁵ cells/ml for MCF-7 followed by 24 h of incubation. The effect of the vehicle solvent (DMSO) on the growth of these cell lines was evaluated in all the experiments by exposing untreated control cells to the maximum concentration (0.5%) of DMSO used in each assay. The activity of the compounds was evaluated using sulforhodamine B dye where cells were treated with five different serial dilutions (up to 150 µM) of the compounds for 48 h. Doxorubicin was used as a positive control and tested in the same manner. The cytotoxicity of the compounds were then determined using the SRB method as previously described by Skehan et al. [53]. Similarly, compound **17** was tested on the triple negative human tumor breast cancer cell MDA-MB-231 and on the normal breast cell line MCF-10A.

A-549 human lung cancer cell line were grown in DMEM supplemented with 10% heat inactivated FBS, 50 units/ml of penicillin

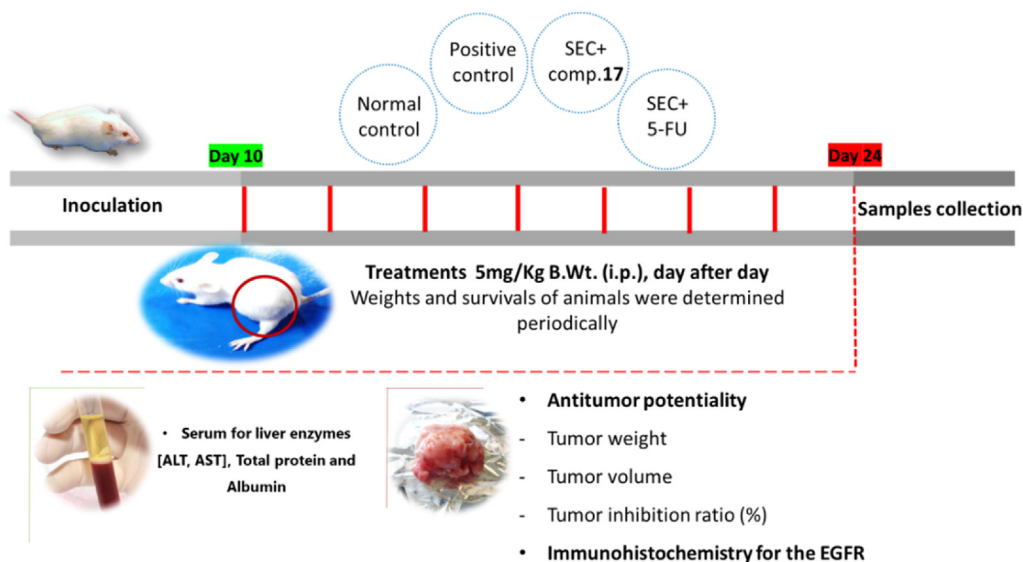


Fig. 12. *In vivo* experimental design [56].

and 50 mg/ml of streptomycin and maintained at 37 °C in a humidified atmosphere containing 5% CO₂. The cells were maintained as monolayer culture by serial subculturing. The cytotoxicity of the compounds were then determined using the SRB method as previously described by Skehan et al. [53]. The IC₅₀ values were calculated according to the equation for Boltzman sigmoidal fitting models (Graph Pad, Prism Version 5).

4.2.2. Investigation of apoptosis by annexin V/PI staining and cell cycle analysis

Apoptosis rate in cells was quantified using annexin V-FITC (BD Pharmingen, USA). Cells were seeded into 6-well culture plates (3–5 × 10⁵ cells/well) and incubated for an overnight. Cells were then treated with compound **17** for 48 h at its IC₅₀ value concentration. Next, media supernatants and cells were collected and rinsed with ice-cold PBS. Next, the cells were suspended in 100 µL of annexin binding buffer solution “25 mM CaCl₂, 1.4 M NaCl, and 0.1 M HEPES/NaOH, pH 7.4” and incubated with annexin V-FITC solution (1:100) and propidium iodide (PI) at a concentration of 10 µg/mL” in the dark for 30 min. Stained cells were then acquired by Cytoflex FACS machine. Data was analyzed using cytExpert software [54–56].

4.2.3. Real time-polymerase chain reaction for the selected genes

To further investigate the apoptotic pathway, we followed the gene expression of P53, Bax, PUMA, Caspases-3, 8 and 9 as proapoptotic genes and BCL2 as the anti-apoptotic gene; their sequences in forward and reverse direction were provided in the supplementary data. MCF-7 cells were treated with compound **17** at its IC₅₀ value for 48 h. After completing the treatment period, cells were collected and total RNA was extracted using Rneasy® Mini Kit (Qiagen, Hilden, Germany). Then, cDNA was synthesized using 500 ng of RNA (*i*-Script cDNA synthesis kit, BioRad, Hercules, USA). Finally, each RT-PCR reaction was performed using 25 µL of Fluocycle®II SYBR® (Euroclone Milan, Italy), 10 ng of cDNA and 2 µL of 10 µM for forward and reverse primers. We completed the reaction mix by adding 19 µL of nuclease free water. All reactions were performed for 35 cycles using the following temperature profiles: 95 °C for 5 min (initial denaturation); 95 °C for 15 min (Denaturation), 55 °C for 30 min (Annealing), and 72 °C for 30 min (Extension). Then, the Ct values were collected for calculation of the

relative genes' expression in all samples by normalization to the β-actin housekeeping gene [54,57].

4.3. In vivo experiment

The experimental protocol was approved by the Research Ethics Committee at Suez Canal University (Approval number REC-07-2020, Faculty of Science, Suez Canal University). *In vivo* experiments were conducted as illustrated in Fig. 12.

4.4. Autophagy evaluation using acridine orange quantitative assessment

Autophagic cell death is quantitatively assessed using acridine orange lysosomal stain coupled with flowcytometric analysis. After treatment with test compound for 48h, MCF-7 cells (10⁵ cells) were collected by trypsinization and washed twice with ice-cold PBS (pH 7.4). Cells were stained with acridine orange (10 µM) and incubated in the dark at 37 °C for 30 min. After staining, cells were injected into ACEA Novocyte™ flowcytometer (ACEA Biosciences Inc., San Diego, CA, USA) and acridine orange fluorescent signals was analyzed using FL1 signal detector (λ_{ex/em} 488/530 µM). For each sample, 12,000 events were acquired and net fluorescent intensities (NFI) were quantified using ACEA NovoExpress™ software (ACEA Biosciences Inc., San Diego, CA, USA).

4.5. EGFR PK inhibition

EGFR-TK cell-free assay was used to explore the effect on the test compounds on inhibition of EGFR kinase according to the reported method. The autophosphorylation percentage inhibition was calculated using the following equation:
$$100 - \left[\frac{\text{Control}}{\text{Treated}} - \text{Control} \right]$$
 IC₅₀ was calculated from the curves of percentage inhibition of five concentrations (0.01, 0.1, 1, 10 and 100 µM) for each compound, using GraphPad prism7 software [58].

4.6. Molecular docking

Both protein and ligand structures were optimized, and energetically favored using Maestro. Molecular docking study towards EGFR protein (PDB = 1M17) was performed using MOE version

2019.01 following routine work [54] of preparation of the appropriate formats of receptor and ligands. Grid box dimensions were determined for a box of 10 Å in the x, y and z directions centered on the ligand. Finally, docking was performed using default parameters and S scores were recorded. Chimera was used to analyze the binding disposition and interactive modes.

Declaration of competing interest

The authors declare that they have no known competing financial interests or personal relationships that could have appeared to influence the work reported in this paper.

Appendix A. Supplementary data

Supplementary data to this article can be found online at <https://doi.org/10.1016/j.ejmech.2021.113609>.

References

- [1] D.S. Shewach, R.D. Kuchta, Introduction to cancer chemotherapeutics, *Chem. Rev.* 109 (2009) 2859–2861.
- [2] R. Bansal, A. Malhotra, Therapeutic progression of quinazolines as targeted chemotherapeutic agents, *Eur. J. Med. Chem.* 211 (2021), 113016.
- [3] V. Sharma, R. Kamal, V. Kumar, Heterocyclic analogues as kinase inhibitors: a focus review, *Curr. Top. Med. Chem.* 17 (2017) 2482–2494.
- [4] J. Zhang, P.L. Yang, N.S. Gray, Targeting cancer with small molecule kinase inhibitors, *Nat. Rev. Canc.* 9 (2009) 28–39.
- [5] S. Kobayashi, T.J. Boggon, T. Dayaram, P.A. Jänne, O. Kocher, M. Meyerson, B.E. Johnson, M.J. Eck, D.G. Tenen, B. Halmos, EGFR mutation and resistance of non-small-cell lung cancer to gefitinib, *N. Engl. J. Med.* 352 (2005) 786–792.
- [6] A. Thakur, G.J. Tawa, M.J. Henderson, C. Danchik, S. Liu, P. Shah, A.Q. Wang, G. Dunn, M. Kabir, E.C. Padilha, X. Xu, A. Simeonov, S. Kharbanda, R. Stone, G. Grewal, Design, synthesis, and biological evaluation of quinazolin-4-one-based hydroxamic acids as dual PI3K/HDAC inhibitors, *J. Med. Chem.* 63 (2020) 4256–4292.
- [7] G.V. De Lucca, Q. Shi, Q. Liu, D.G. Batt, M. Beaudoin Bertrand, R. Rampulla, A. Mathur, L. Disenza, C. D'Arienzo, J. Dai, M. Obermeier, R. Vickery, Y. Zhang, Z. Yang, P. Marathe, A.J. Tebben, J.K. Muckelbauer, C.J. Chang, H. Zhang, K. Gillooly, T. Taylor, M.A. Pattoli, S. Skala, D.W. Kukral, K.W. McIntyre, L. Salter-Cid, A. Fura, J.R. Burke, J.C. Barrish, P.H. Carter, J.A. Tino, Small molecule reversible inhibitors of bruton's tyrosine kinase (BTK): structure–activity relationships leading to the identification of 7-(2-Hydroxypropan-2-yl)-4-[2-methyl-3-(4-oxo-3,4-dihydroquinazolin-3-yl)phenyl]-9H-carbazole-1-carboxamide (BMS-935177), *J. Med. Chem.* 59 (2016) 7915–7935.
- [8] J. Dong, J. Huang, J. Zhou, Y. Tan, J. Jin, X. Tan, B. Wang, T. Yu, C. Wu, S. Chen, T.-L. Wang, Discovery of 3-quinazolin-4(3H)-on-3-yl-2,N-dimethylpropanamides as orally active and selective PI3K α inhibitors, *ACS Med. Chem. Lett.* 11 (2020) 1463–1469.
- [9] L. Hudson, J. Mui, S. Vázquez, D.M. Carvalho, E. Williams, C. Jones, A.N. Bullock, S. Hoelder, Novel quinazolinone inhibitors of ALK2 flip between alternate binding modes: structure–activity relationship, structural characterization, kinase profiling, and cellular proof of concept, *J. Med. Chem.* 61 (2018) 7261–7272.
- [10] S. Perreault, J. Chandrasekhar, Z.-H. Cui, J. Everts, J. Hao, J.A. Kaplan, A. Kashishian, K.S. Keegan, T. Kenney, D. Koditek, L. Lad, E.-I. Lepist, M.E. McGrath, L. Patel, B. Phillips, J. Therrien, J. Treiberg, A. Yahiaoui, G. Phillips, Discovery of a phosphoinositide 3-kinase (PI3K) β/δ inhibitor for the treatment of phosphatase and tensin homolog (PTEN) deficient tumors: building PI3K β potency in a PI3K δ -selective template by targeting non-conserved Asp856, *J. Med. Chem.* 60 (2017) 1555–1567.
- [11] C.-W. Yu, P.-Y. Hung, H.-T. Yang, Y.-H. Ho, H.-Y. Lai, Y.-S. Cheng, J.-W. Chern, Quinazolin-2,4-dione-Based hydroxamic acids as selective histone deacetylase-6 inhibitors for treatment of non-small cell lung cancer, *J. Med. Chem.* 62 (2019) 857–874.
- [12] C.W. Yun, S.H. Lee, The roles of autophagy in cancer, *Int. J. Mol. Sci.* 19 (2018), 3466.
- [13] S.K. Yeo, J. Wen, S. Chen, J.-L. Guan, Autophagy differentially regulates distinct breast cancer stem-like cells in murine models via EGFR/Stat3 and tgfb/smad signaling, *Canc. Res.* 76 (2016) 3397–3410.
- [14] E. White, Deconvoluting the context-dependent role for autophagy in cancer, *Nat. Rev. Canc.* 12 (2012) 401–410.
- [15] V. Karantza, S. Patel, O. Kravchuk, G. Chen, R. Mathew, S. Jin, E. White, Autophagy mitigates metabolic stress and genome damage in mammary tumorigenesis, *Gene Dev.* 21 (2007) 1621–1635.
- [16] H. Wei, S. Wei, B. Gan, X. Peng, W. Zou, J.L. Guan, Suppression of autophagy by FIP200 deletion inhibits mammary tumorigenesis, *Genes Dev.* 25 (2011) 1510–1527.
- [17] H.-A. Ha, J.-H. Chiang, F.-J. Tsai, D.-T. Bau, Y.-N. Juan, Y.-H. Lo, M.-J. Hour, J.-S. Yang, Novel quinazolinone MJ-33 induces AKT/mTOR-mediated autophagy-associated apoptosis in 5FU-resistant colorectal cancer cells, *Oncol. Rep.* 45 (2020) 680–692.
- [18] S. Kumar, S.K. Guru, A.S. Pathania, N. Mupparapu, A. Kumar, F. Malik, S.B. Bharate, Q. Naveed Ahmed, R.A. Vishwakarma, S. Bhushan, A novel quinazolinone derivative induces cytochrome c interdependent apoptosis and autophagy in human leukemia MOLT-4 cells, *Toxicol. Reports* 1 (2014) 1013–1025.
- [19] X. Liu, P. Zhao, X. Wang, L. Wang, Y. Zhu, W. Gao, Triptolide induces glioma cell autophagy and apoptosis via upregulating the ROS/JNK and down-regulating the akt/mTOR signaling pathways, *Front Oncol* 9 (2019), 387–387.
- [20] P. Zhang, Z. Zheng, L. Ling, X. Yang, N. Zhang, X. Wang, M. Hu, Y. Xia, Y. Ma, H. Yang, Y. Wang, H. Liu, w09, a novel autophagy enhancer, induces autophagy-dependent cell apoptosis via activation of the EGFR-mediated RAS-RAF1-MAP2K-MAPK1/3 pathway, *Autophagy* 13 (2017) 1093–1112.
- [21] L. Booth, M. Tavallai, H. Hamed, N. Cruickshanks, P. Dent, The role of cell signalling in the crosstalk between autophagy and apoptosis, *Cell. Signal.* (2013) 26.
- [22] C. Fung, X. Chen, J.R. Grandis, U. Duvvuri, EGFR tyrosine kinase inhibition induces autophagy in cancer cells, *Canc. Biol. Ther.* 13 (2012) 1417–1424.
- [23] S. Shen, O. Kepp, M. Michaud, I. Martins, H. Minoux, D. Metivier, M.C. Maiuri, R.T. Kroemer, G. Kroemer, Association and dissociation of autophagy, apoptosis and necrosis by systematic chemical study, *Oncogene* 30 (2011) 4544–4556.
- [24] X. Sui, R. Chen, Z. Wang, Z. Huang, N. Kong, M. Zhang, W. Han, F. Lou, J. Yang, Q. Zhang, X. Wang, C. He, H. Pan, Autophagy and chemotherapy resistance: a promising therapeutic target for cancer treatment, *Cell Death Dis.* 4 (2013), e838.
- [25] A. Thorburn, D.H. Thamm, D.L. Gustafson, Autophagy and cancer therapy, *Mol. Pharmacol.* 85 (2014) 830–838.
- [26] M. Ye, S. Wang, T. Wan, R. Jiang, Y. Qiu, L. Pei, N. Pang, Y. Huang, Y. Huang, Z. Zhang, L. Yang, Combined inhibitions of glycolysis and AKT/autophagy can overcome resistance to EGFR-targeted therapy of lung cancer, *J. Canc.* 8 (2017) 3774–3784.
- [27] Y. Kwon, M. Kim, H.S. Jung, Y. Kim, D. Jeoung, Targeting autophagy for overcoming resistance to anti-EGFR treatments, *Cancers* (2019) 11.
- [28] N.H. Elghazawy, A. Hefnawy, N.K. Sedky, I.M. El-Sherbiny, R.K. Arafa, Preparation and nanoformulation of new quinolone scaffold-based anticancer agents: enhancing solubility for better cellular delivery, *Eur. J. Pharmaceut. Sci. : Off. J. Euro. Feder. Pharm. Sci.* 105 (2017) 203–211.
- [29] N.A. El Sayed, A.A. Eissa, G.F. El Masry, Mohamed M. Abdullah, R.K. Arafa, Discovery of novel quinazolinones and their acyclic analogues as multi-kinase inhibitors: design, synthesis, SAR analysis and biological evaluation, *RSC Adv.* 6 (2016) 111767–111786.
- [30] N.A. El-Sayed, M.S. Nour, M.A. Salem, R.K. Arafa, New oxadiazoles with selective-COX-2 and EGFR dual inhibitory activity: design, synthesis, cytotoxicity evaluation and in silico studies, *Eur. J. Med. Chem.* 183 (2019), 111693.
- [31] M.A. Ismail, M.M. Youssef, R.K. Arafa, S.S. Al-Shihry, W.M. El-Sayed, Synthesis and antiproliferative activity of monocationic arylthiophene derivatives, *Eur. J. Med. Chem.* 126 (2017) 789–798.
- [32] R.K. Arafa, M.S. Nour, N.A. El-Sayed, Novel heterocyclic-fused pyrimidine derivatives: synthesis, molecular modeling and pharmacological screening, *Eur. J. Med. Chem.* 69 (2013) 498–507.
- [33] M.M. Youssef, R.K. Arafa, M.A. Ismail, Synthesis, antimicrobial, and antiproliferative activities of substituted phenylfuranyl nicotinamides, *Drug Des. Dev. Ther.* 10 (2016) 1133–1146.
- [34] R.K. Arafa, M.S. Nour, N.A. El-Sayed, Novel heterocyclic-fused pyrimidine derivatives: synthesis, molecular modeling and pharmacological screening, *Eur. J. Med. Chem.* 69 (2013) 498–507.
- [35] H.S.A. El-Zahabi, M.M.A. Khalifa, Y.M.H. Gado, A.M. Farrag, M.M. Elaasser, N.A. Safwat, R.R. AbdelRaouf, R.K. Arafa, New thiobarbituric acid scaffold-based small molecules: synthesis, cytotoxicity, 2D-QSAR, pharmacophore modelling and in-silico ADME screening, *Eur. J. Pharmaceut. Sci.* 130 (2019) 124–136.
- [36] A.S. Wheeler, W.M. Oates, The bromination OF anthranilic acid, *J. Am. Chem. Soc.* 32 (1910) 770–773.
- [37] V. Alagarsamy, G. Muruganathan, R. Venkateshperrumal, Synthesis, analgesic, anti-inflammatory and antibacterial activities of some novel 2-methyl-3-substituted quinazolin-4(3H)-ones, *Biol. Pharm. Bull.* 26 (2003) 1711–1714.
- [38] F.K. Mohammed, H.M. Bakeer, M.A. El-Hashash, Studies on 2-substituted-6,8-dibromo-4(H)-3,1-benzoxazin-4-one, *Asian J. Chem.* 21 (2009) 5004–5014.
- [39] A.R. Desai, K.R. Desai, Niementowski Reaction: Microwave Induced and Conventional Synthesis of Quinazolinones and 3-Methyl-1h-5-Pyrazolones and Their Antimicrobial Activity, *ARKIVOC*, Gainesville, FL, U. S., 2005, pp. 98–108.
- [40] H.A. Saad, N.A. Osman, A.H. Moustafa, Synthesis and analgesic activity of some new pyrazoles and triazoles bearing a 6,8-dibromo-2-methylquinazoline moiety, *Molecules* 16 (2011) 10187–10201.
- [41] M.J. Abedin, D. Wang, M.A. McDonnell, U. Lehmann, A. Kelekar, Autophagy delays apoptotic death in breast cancer cells following DNA damage, *Cell Death Differ.* 14 (2007) 500–510.
- [42] A. El Guerrab, M. Bamdad, Y.J. Bignon, F. Penault-Llorca, C. Aubel, Co-targeting EGFR and mTOR with gefitinib and everolimus in triple-negative breast cancer cells, *Sci. Rep.* 10 (2020) 6367.

- [43] S. Glaysher, L.M. Bolton, P. Johnson, C. Torrance, I.A. Cree, Activity of EGFR, mTOR and PI3K inhibitors in an isogenic breast cell line model, *BMC Res. Notes* 7 (2014) 397.
- [44] J.C. Soria, P. LoRusso, R. Bahleda, J. Lager, L. Liu, J. Jiang, J.F. Martini, S. Mace, H. Burris, Phase I dose-escalation study of pialaralisib (SAR245408, XL147), a pan-class I PI3K inhibitor, in combination with erlotinib in patients with solid tumors, *Oncol.* 20 (2015) 245–246.
- [45] M.F. Zayed, H.S. Rateb, S. Ahmed, O.A. Khaled, S.R.M. Ibrahim, Quinazolinone-amino acid hybrids as dual inhibitors of EGFR kinase and tubulin polymerization, *Molecules* 23 (2018).
- [46] Y. Le, Y. Gan, Y. Fu, J. Liu, W. Li, X. Zou, Z. Zhou, Z. Wang, G. Ouyang, L. Yan, Design, synthesis and in vitro biological evaluation of quinazolinone derivatives as EGFR inhibitors for antitumor treatment, *J. Enzym. Inhib. Med. Chem.* 35 (2020) 555–564.
- [47] Zaranappa, M.S. Niranjana, K.C. Chaluvajuru, H.M. Vagdevi, Synthesis and antihypertensive activity of 6, 8- dibromo-3-phenyl-2-substituted styryl-quinazolin-4(3h), *ones* 4 (2012) 1861–1865.
- [48] H. Madkour, Behaviour of dynamic 6,8-dibromo-2-methyl-4-(H)-3, 1-benzoxazin-4-one towards some nitrogen nucleophiles: synthesis of new quinazolinones with anticipated biological activity, *J. Org. Chem.* 4 (2008).
- [49] A.M. Reddy, G. Ramamurthy, V.M. Reddy, K. Mogilaiah, Synthesis of 3-(4-aryl-3-mercapto-4H-1,2,4-triazol-5-ylmethyl)-2-methyl-4(3H)quinazolinones, *Sulfur Lett.* 8 (1988) 1–9.
- [50] A.M. Reddy, G. Achaiiah, A.D. Rao, V.M. Reddy, Synthesis of 2-methyl-4-oxo-N-(4-oxo-2-arylthiazolidin-3-yl)-3(4H)-quinazolineacetamides, *Indian J. Chem., Sect. B* 27B (1988) 1054–1056.
- [51] W. Wei, L. Zhu, Y. Zhou, Z. Li, Synthesis and bioactivities evaluation of novel N-pyridylpyrazole derivatives with 1,2,3-triazole and quinazolin-4(3H)-one substructure, *Heterocycles* 96 (2018) 1453–1462.
- [52] O.O. Peter, O.O. Lucky, Design, synthesis and bioassay of novel metal complexes of 3-amino-6,8-dibromo-2-methyl quinazolin-4(3H)-One, *Pharmaceut. Chem. J.* 48 (2015) 718–721.
- [53] P. Skehan, R. Storeng, D. Scudiero, A. Monks, J. McMahon, D. Vistica, J.T. Warren, H. Bokesch, S. Kenney, M.R. Boyd, New colorimetric cytotoxicity assay for anticancer-drug screening, *J. Natl. Cancer Inst.* 82 (1990) 1107–1112.
- [54] M.S. Nafie, K. Arafa, N.K. Sedky, A.A. Alakhdar, R.K. Arafa, Triaryl dicationic DNA minor-groove binders with antioxidant activity display cytotoxicity and induce apoptosis in breast cancer, *Chem. Biol. Interact.* 324 (2020), 109087.
- [55] M.S. Nafie, A.M. Amer, A.K. Mohamed, E.S. Tantawy, Discovery of novel pyrazolo[3,4-b]pyridine scaffold-based derivatives as potential PIM-1 kinase inhibitors in breast cancer MCF-7 cells, *Bioorg. Med. Chem.* 28 (2020), 115828.
- [56] E.M. Gad, M.S. Nafie, E.H. Eltamany, M. Hammad, A. Barakat, A.T.A. Boraei, Discovery of new apoptosis-inducing agents for breast cancer based on ethyl 2-amino-4,5,6,7-tetra hydrobenzo[b]Thiophene-3-carboxylate: synthesis, in vitro, and in vivo activity evaluation, *Molecules* (2020) 25.
- [57] M.S. Nafie, S. Mahgoub, A. Amer, Antimicrobial and antiproliferative activities of novel synthesized 6-(quinolin-2-ylthio) pyridine derivatives with molecular docking study as multi-targeted JAK2/STAT3 inhibitors, *Chem. Biol. Drug Des.* 97 (2021) 553–564.
- [58] M. Hisham, B.G.M. Youssif, E.E.A. Osman, A.M. Hayallah, M. Abdel-Aziz, Synthesis and biological evaluation of novel xanthine derivatives as potential apoptotic antitumor agents, *Eur. J. Med. Chem.* 176 (2019) 117–128.